

Two-dimensional materials for tunable and nonlinear metaoptics

Zeng Wang,[†] Kandammathe Valiyaveedu Sreekanth,[†] Meng Zhao,[†] Jinpeng Nong, Yincheng Liu[✉], and Jinghua Teng^{✉*}

Agency for Science, Technology and Research (A*STAR), Institute of Materials Research and Engineering (IMRE), Singapore

Abstract. Metaoptics formed by ultrathin and planar building blocks enable compact and efficient optical devices that manipulate light at the nanoscale. The development of tunable metaoptics holds the promise of miniaturized and efficient optical systems that can dynamically adapt to changing conditions or requirements, propelling innovations in fields ranging from telecommunication and imaging to quantum computing and sensing. Two-dimensional (2D) materials show strong promise in enabling tunable metaoptics due to their exceptional electronic and optical properties from the quantum confinement within the atomically thin layers. In this review, we discuss the recent advancements and challenges of 2D material-based tunable metaoptics in both linear and nonlinear regimes and provide an outlook for prospects in this rapidly advancing area.

Keywords: metaoptics; tunable metaoptics; two-dimensional optoelectronics; nonlinear optics; excitons; polaritons.

Received Dec. 13, 2023; revised manuscript received Mar. 28, 2024; accepted for publication Apr. 18, 2024; published online May 20, 2024.

© The Authors. Published by SPIE and CLP under a Creative Commons Attribution 4.0 International License. Distribution or reproduction of this work in whole or in part requires full attribution of the original publication, including its DOI.

[DOI: [10.1117/1.AP.6.3.034001](https://doi.org/10.1117/1.AP.6.3.034001)]

1 Introduction

The advent of flat optics or metaoptics heralds a significant transformation in optical technology, blending with the pursuit of replacing traditional bulky optical components with planar and compact alternatives.^{1–4} It is bringing revolution not only to optics design and functionality but also to ways of manufacturing optics and related optical systems for applications^{5–10} such as optical communication, imaging, and sensing. Despite rapid progress in metaoptics, the insignificant changes in the complex permittivity in their building blocks made of metals, dielectrics, or bulk semiconductors under external influences limit the approaches to tune their plasmonic or Mie resonance, thereby undermining their potential for dynamic light control that could bring forth many new phenomena and applications. Various tunable and reconfigurable metaoptics based on different materials and mechanisms have been investigated,^{5,11,12} including liquid crystals^{13–15} and phase change materials^{16–19} that demonstrated relatively large refractive index tuning under electrical control. Two-dimensional (2D) materials show extraordinary potential from their exceptional electronic and optical characteristics

shaped by quantum confinement within a few atoms' thickness, which led to distinctive excitonic effects not found in bulk materials.^{20–22}

The tunability of excitonic resonance in 2D materials has emerged as a possible avenue for the next generation of ultrathin metaoptics.^{23–26} For example, the reduced dielectric screening in atomically thin transition metal dichalcogenides (TMDCs) enhances exciton binding energies, surpassing the room temperature (RT) thermal energy of ~ 0.026 eV. This results in robust excitons in TMDCs and creates a versatile platform for manipulating exciton resonance through strong light–matter interaction to enable dynamics and wide-range complex refractive index control.^{27,28} In addition to neutral excitons, recent research has uncovered a variety of closely associated quasi-particles, such as charged excitons or trions, which also play a significant role in 2D systems.^{29–34} These quasi-particles notably impact the system's tunability up to RT, a phenomenon uncommon in bulk semiconductors. The coexistence of excitons and trions is particularly influential for 2D tunable metaoptics, as it directly alters the optical properties of these systems. Consequently, a thorough understanding of trionic behavior is essential for achieving optimal performance in such devices.

In the near field, the highly tunable polaritons in 2D materials offer a concrete avenue to surpass the diffraction limit and

*Address all correspondence to Jinghua Teng, jh-teng@imre.a-star.edu.sg

[†]These authors contributed equally to the work.

achieve light manipulation in extremely confined space. Polaritons are a class of quasi-particles that originate from the coupling between photons and collective excitations. For example, plasmon polaritons are formed when the collective oscillation of electrons in metals, i.e., plasmons, is coupled with photons, while phonon polaritons (PhPs) are formed when collective lattice vibrations, i.e., phonons, are coupled with photons. 2D polaritons are believed to hold tremendous potential in advancing nanophotonics because of their high susceptibility to external stimuli. Surface plasmon polaritons in graphene have been extensively studied for their strong light-field confinement and good tunability in the mid–far infrared (IR) range,^{35,36} and PhPs with hyperbolic dispersion in structured graphene, hexagonal boron nitride (h-BN), and other 2D materials have been used to demonstrate hyperbolic metasurfaces.^{37–39} What makes 2D polaritons even more intriguing is that the topological and quantum states in 2D materials open new opportunities to understand, engineer, and utilize polaritons in 2D materials.

Besides the linear regime, metaoptics have recently emerged as a promising platform to study the nonlinear optical phenomena bearing the merits of loosened phase-matching requirements in the subwavelength dimension, strongly enhanced light–matter interaction due to field confinement or high- Q resonance, and the much smaller light interaction scale than the light coherence length.^{40–45} The large nonlinear optical coefficients discovered in 2D materials, besides the tunable exciton and polariton resonance, the broadband optical response, and strong interlayer coupling, make 2D materials natural candidates for nonlinear optics.^{46–50} Integrating metaoptics with 2D materials holds immense potential for significantly enhancing and even tuning nonlinear effects, paving the way for the discovery of novel phenomena and more efficient applications.

This review explores the cutting-edge developments in the unique excitonic and polaritonic effects in 2D materials and their significant impact on metaoptics. It delves into the basic physics underlying excitons and quasi-particles in 2D materials, highlights the progress in metaoptics driven by the tunability of excitonic resonance, especially for TMDCs working in the visible range, and examines the creative methods employed to incorporate 2D materials into adaptable optical applications. It further discusses, in particular, tunable polaritons in manipulating and enhancing light–matter interactions in highly confined space in materials such as graphene and TMDCs. It also highlights the nonlinear optical properties of these materials, accentuating their potential in creating ultracompact and energy-efficient optoelectronic components. The synergy of these nonlinear phenomena with the versatile electronic and mechanical properties of 2D materials, particularly when integrated into heterostructures, opens new avenues for the development of advanced photonic and optoelectronic systems with customizable and dynamic functionalities. By examining both the current challenges and future research arenas, this review seeks to offer insights into the utilization of 2D materials for creating a novel category of tunable metaoptics, with the potential of transforming the field of optical technologies.

2 2D Excitons for Tunable Metaoptics

2.1 Fundamentals of Excitons in 2D Materials

Excitons are quasi-particles consisting of an electron and a hole bound together by their electrostatic Coulomb attraction. They

play a crucial role in the optical and electronic properties of 2D materials, particularly in TMDCs. Due to strong spatial confinement and reduced dielectric screening, their binding energies are significantly higher than those in bulk materials.⁵¹ In three-dimensional (3D) semiconductors, the exciton binding energy (E_b) could be estimated using the hydrogen model below when neglecting the quantum defect,

$$E_b^{3D}(n) = \frac{R_Y}{n^2}.$$

Here, R_Y is the Rydberg constant for excitons, and n is the quantum number. In two dimensions, due to the quantum confinement influencing the exciton radius and average dielectric constant, the Rydberg exciton binding energy is modified as

$$E_b^{2D}(n) = \frac{R_Y}{(n - \frac{1}{2})^2}.$$

This implies that the lowest 2D exciton binding energy ($n = 1$) has a magnitude 4 times larger than the 3D one at ground state, as demonstrated in Figs. 1(a) and 1(b). Experimentally, binding energies of excitons can range from a few hundred meV to over 1 eV in 2D materials, as shown in Fig. 1(c). For example, the A exciton in monolayer MoS₂ has a binding energy of ~ 0.5 eV, which is substantially greater than the thermal energy at RT (26 meV) and the binding energies of typical bulk semiconductors such as GaAs (~ 15 meV). Therefore, excitons are highly stable in monolayer TMDCs, even at RT. It is important to note that the reported binding energy values for the same material can differ significantly across various studies due to differences in material quality, the dielectric environment, experimental conditions, and other factors.

Compared with neutral excitons, trions in 2D TMDCs are more complex quasi-particles involving two electrons and one hole or two holes and one electron bound together, forming negatively or positively charged excitons, respectively, as illustrated in Fig. 2(a). The presence of trions significantly influences the optical properties of TMDCs. When discussing trions, it is also essential to consider their binding energy, which is typically much lower than that of neutral excitons due to the additional electron or hole.^{34,51,52} The binding energy of trions can be estimated by considering the additional electron–hole Coulomb interaction and is expressed as $E_{\text{binding trion}} = E_{\text{exciton}} - E_{\text{trion}}$. It is indeed worth noting that the observation of trion binding energy is very limited due to the difficulties in obtaining accurate and reliable measurements of reflectance in ultrathin samples under doping from the weak light–matter interaction. Among various reports,^{53–55} a direct absorption measurement estimated WS₂ trion binding energy around 31 to 37 meV at 5 K based on h-BN encapsulated samples, as shown in Figs. 2(b)–2(d),⁵⁶ and another study using reflectance contrast spectra reported the zero-density trion binding energy of 23 meV at 50 K.⁵⁷ Thanks to the cavity effect, Wang et al.⁵⁸ recently determined the trion binding energy via the reflectance at RT to be around 42 meV in slightly n-doped condition, and they estimated the trion binding energy to be around 34 meV in the zero-density at zero bias by extrapolating the linearly fitted trion binding energies under different voltages, as shown in Figs. 2(e) and 2(f).

The impact of trions on tunable metaoptics is profound. The tunability comes from the ability to control the charge carrier

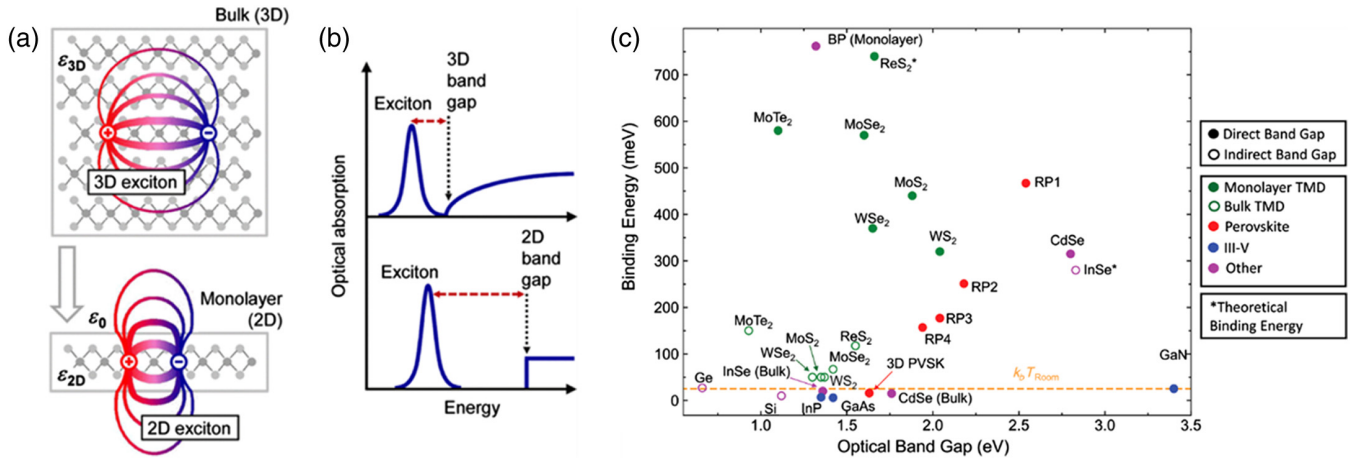


Fig. 1 (a) Electrons and holes bound into excitons for the 3D bulk and 2D materials. (b) The transition from 3D to 2D is expected to lead to an increase of both the bandgap and the exciton binding energy (indicated by the dashed red line). (c) Binding energy of excitons in some common 3D and 2D semiconductors. The yellow dotted line represents the thermal energy at RT. Panels (a) and (b) were reproduced with permission from Ref. 51 © 2014—APS, and panel (c) was reproduced with permission from Ref. 52 © 2022—AIP.

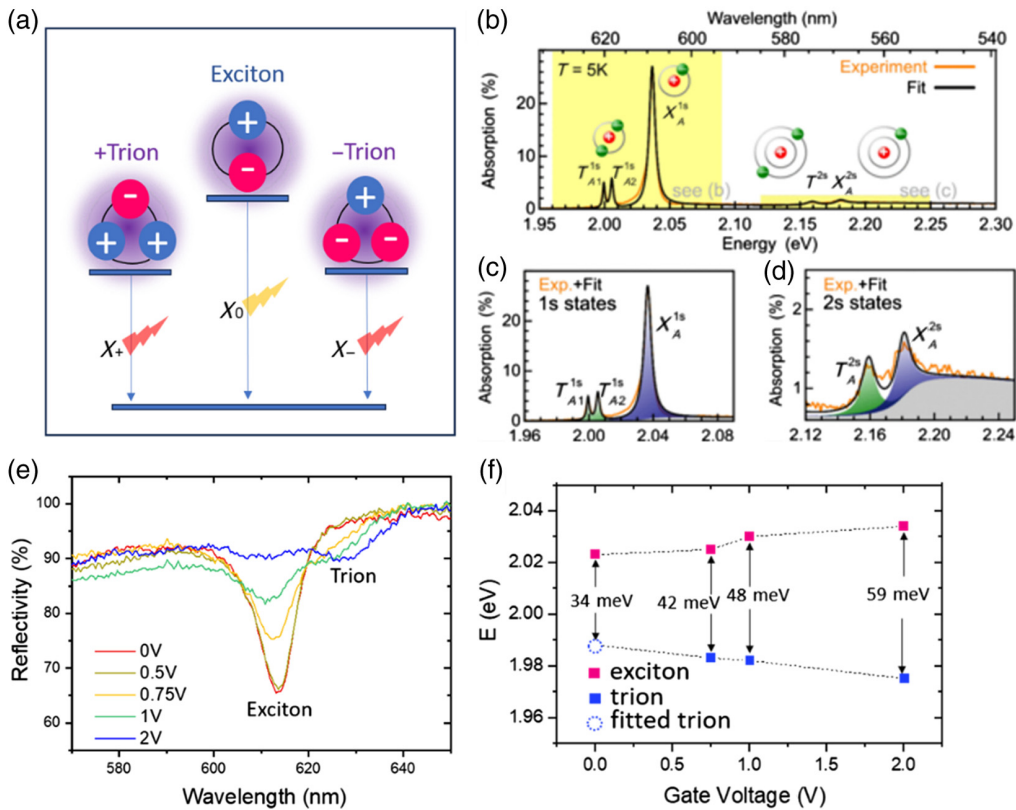


Fig. 2 (a) Illustration of the exciton and trion. (b) Optical absorption spectrum of an h-BN-encapsulated WS₂ monolayer measured at $T = 5$ K. (c) Experimental and fitted spectra for $n = 1$ states, where shaded green and blue regions represent the contributions from trions and excitons, respectively. (d) Zoomed-in view highlighting ($n = 2$) excited state trions and excitons. (e) Cavity-enhanced exciton-trion resonance at RT. (f) WS₂ trion binding energy measured at RT. Panels (b)–(d) were reproduced with permission from Ref. 56 © 2019—APS, and panels (e) and (f) were reproduced with permission from Ref. 58 © 2023—Wiley.

concentration in TMDCs through gating, doping, or photoexcitation, which directly affects the trion population and, consequently, the optical response of the material. For instance, by applying an electrical field through a gate, one can modulate the free-carrier concentration, thereby switching between exciton and trion resonances. This effect can be used to dynamically control the reflectance, transmittance, and absorption of light in metaoptics, making trions an active element for reconfigurable photonics.

2.2 Excitonic Tunability in 2D Materials for Active Metaoptics

Although the excitonic resonance has strong oscillation strength, the very limited interaction length still results in an insignificant overall optical response. To enhance excitonic resonances, the encapsulation of TMDCs with h-BN under low-temperature working conditions has been adapted for various 2D devices. h-BN encapsulation provides a cleaner, stabler, and protective environment for TMDCs, leading to enhanced excitonic and trionic properties, while operation at low temperatures mitigates phonon scattering and thermal broadening, resulting in sharper excitonic resonances.

In the study of Back et al.,⁵⁹ a single MoSe₂ monolayer was used to create an electrically tunable mirror. As shown in Figs. 3(a)–3(c), MoSe₂ is sandwiched between two layers of h-BN, which acted as a resonant cavity, enhancing light interaction with the excitonic resonance. At around 4 K, exciton

decay became purely radiative, and the encapsulated MoSe₂ flakes showed strong tunable exciton resonance, producing adjustable transmission from 10% to 60%. Zhou et al.⁶⁰ also reported similar results. Very recently, Li et al.⁶¹ advanced the function of h-BN encapsulated MoSe₂ for dynamically steering beams between -30° and 30° via varying gate voltage, displayed in Figs. 3(d)–3(f). Although the demonstrations were on small MoSe₂ flakes at cryogenic temperatures, these initial examples have shown that single-layer TMDCs can attain significant optical efficiencies with the added advantage of electrical manipulation of their optical properties.

Toward realizing practical excitonic metaoptics, it is essential to develop the ability for devices to work at RT. WS₂ has been identified as a promising candidate to maintain the relatively strong oscillator strength of excitons at RT. As shown in Figs. 4(a) and 4(b),⁶² a Fresnel zone plate lens with a diameter of 1 mm is patterned from a large-area monolayer WS₂ grown on sapphire via chemical vapor deposition. This lens has been designed to operate optimally at wavelengths close to the exciton resonance and has a focal length of 2 mm. The 33% active modulation of focusing efficiency has been shown via exciton resonance tuning. Although the absolute absorption tuning is less than 1%, this first demonstration of exciton resonance tuning in large-area TMDCs samples highlights the opportunities that excitons offer for tunable metaoptics. Subsequently, the same group reported enhanced tunability of exciton resonances via metasurface-induced Purcell effect to boost both the excitation field and radiative decay for excitons.⁶³ In Figs. 4(c) and

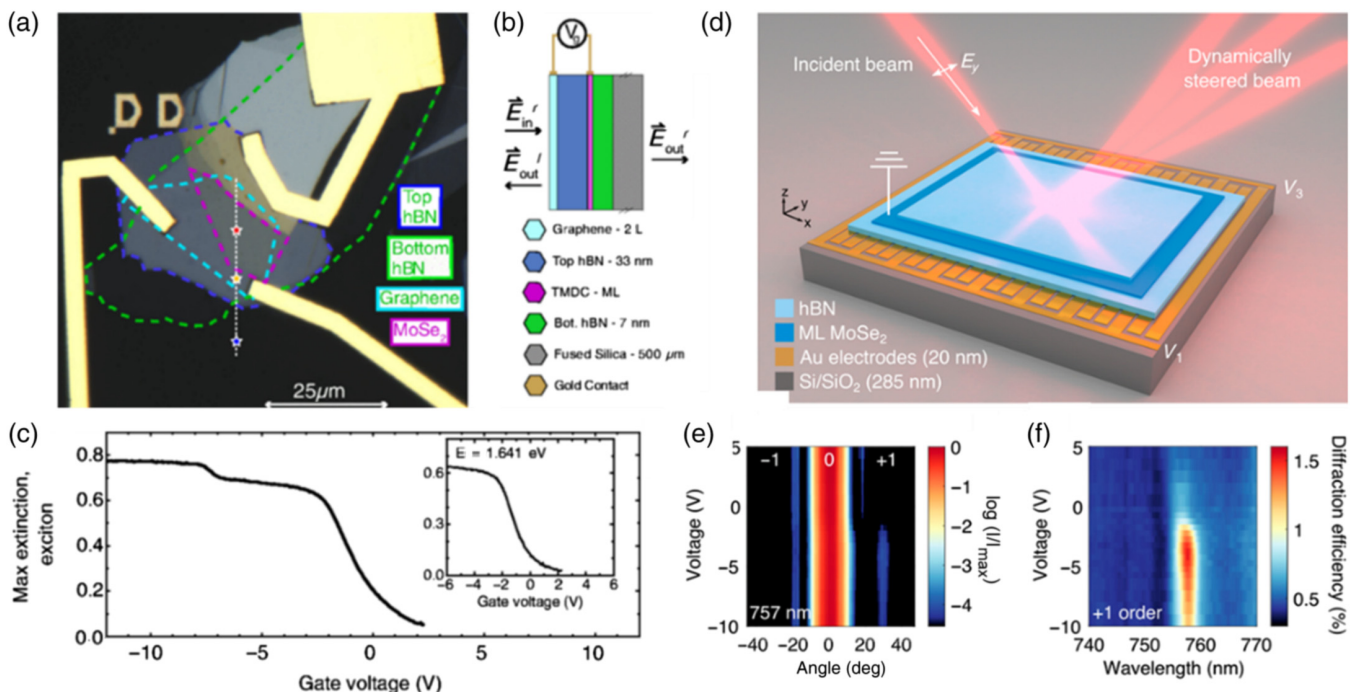


Fig. 3 Excitonic metaoptics working at low temperature. (a) Micrograph of the measured heterostructure. The MoSe₂ monolayer is encapsulated between 33 nm (top) and 7 nm (bottom) thick h-BN layers. (b) Interaction of an incident field with a MoSe₂ monolayer. (c) Gate voltage (V_g) dependence of the maximal extinction of transmitted light using the exciton resonance. (d) Schematic of the exciton-based TMDC metaoptics for dynamic beam steering. (e) Beam steering angle under the applied asymmetric voltage gradient. (f) Voltage and spectral dependence of the diffraction efficiency. Panels (a)–(c) were reproduced with permission from Ref. 59 © 2018—APS, and panels (d)–(f) were reproduced with permission from Ref. 61 © 2023—ACS.

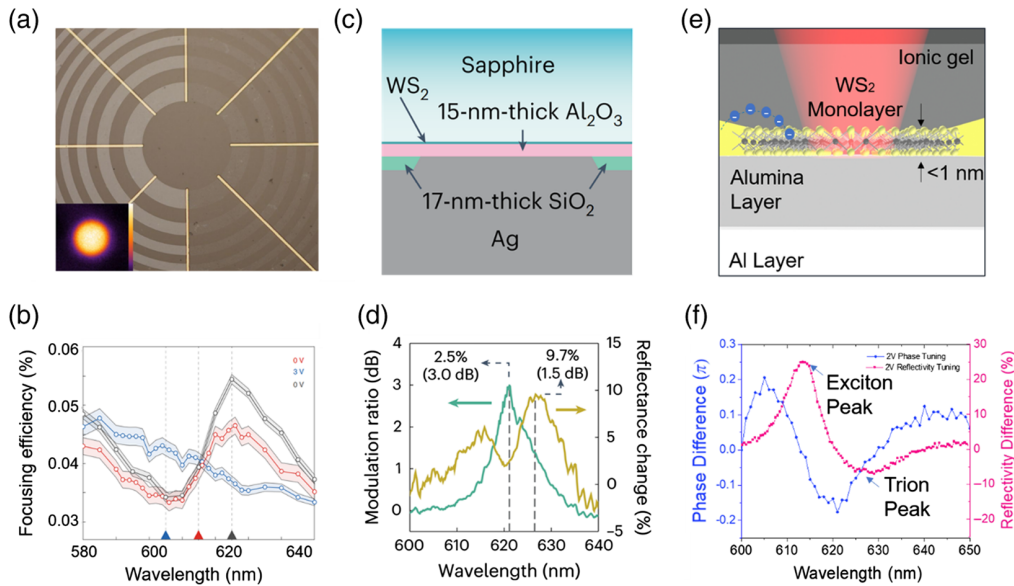


Fig. 4 Excitonic metaoptics working at RT. (a) A Fresnel zone plate lens made on monolayer WS₂. (b) Excitonic modulation of the light intensity in the focusing spot of the WS₂ zone plate lens. (c) A monolayer WS₂ free-space optical modulator based on a MOS capacitor configuration. (d) Modulation ratio (green) and absolute reflectance change (yellow) spectra. A 3 dB modulation ratio and a 10% reflectance change are observed in the experiment. (e) Al/Al₂O₃ cavity effect to enhance the excitonic resonance of monolayer WS₂. (f) Dynamic phase and amplitude tuning with enhanced excitonic and trionic resonances in monolayer WS₂. Panels (a) and (b) were reproduced with permission from Ref. 62 © 2020—Nature, panels (c) and (d) were reproduced with permission from Ref. 63 © 2023—Nature, and panels (e) and (f) were reproduced with permission from Ref. 58 © 2023—Wiley.

4(d), a 10% reflectance change and a 3 dB signal modulation have been demonstrated. In addition to the substantial advancements in utilizing neutral excitonic effects, exploring and capitalizing on the resonance and tunability of trions present an innovative approach in achieving high levels of tunability. Very recently, the issue of insufficient light-matter interaction in trions that has impeded practical observation and application of trionic events has been investigated.⁵⁴ The study presents a solution utilizing an aluminum/alumina (Al/Al₂O₃) optical cavity,⁵⁸ as depicted in Fig. 4(e). This approach overcomes the challenge of weak resonance and high optical losses in TMDCs at RT, specifically concerning trion states. The outcome is a notable electrical modulation in both amplitude and phase for exciton and trion states. Figure 4(f) shows an absolute reflectance change of 25% for excitons and 7% for trions, with phase adjustments of 0.2π for excitons and 0.1π for trions, respectively. The findings reveal that trions play a key role in the electrical tuning of TMDC devices, even at RT.

Tunable excitonic metaoptics are an emerging field with vast potential, yet there are challenges that need to be addressed to realize its full transformative power. One issue is the precise control of the external stimuli required to tune the excitonic properties, as nonuniform electrostatic gating across a large area can result in uneven tuning of the optical properties. Another issue is the inherent narrowband nature of excitonic resonance that limits the operational bandwidth of metaoptics. These characteristics, while beneficial for certain applications requiring high selectivity, restrict the use of excitonic metaoptics in broadband applications. Potential strategies include the use of multiple materials with staggered resonances as well as interlayer

excitons/trionic properties to create broader or multiple resonant peaks. While challenges abound, the field of tunable excitonic metaoptics is full of opportunities and will witness more advancement for the next generation of ultracompact tunable metaoptics in the near future.

3 Tunable Plasmon and PhPs in 2D Materials

Plasmon and PhPs in 2D materials share the commonality of enabling confined and enhanced light-matter interactions at the nanoscale, leading to highly tunable optical properties.⁶⁴ These interactions allow for precise control over light propagation, frequency, and intensity, which is critical for tunable metaoptics.⁶⁵ By leveraging the adjustable nature of plasmon and PhPs in 2D materials, metaoptics can be designed to dynamically modulate light, facilitating advanced functionalities such as phase manipulation, amplitude control, and polarization conversion.⁶⁶ This paves the way for creating tunable and reconfigurable optical devices and systems capable of adapting their responses to changing external conditions, thereby offering a versatile platform for innovative photonic applications in sensing, imaging, and information processing.

3.1 Tunable Plasmon Polaritons

Plasmon polaritons are electromagnetic wave-induced collective electron oscillations at the metal/dielectric interface that enable the manipulation of light-matter interactions beyond the diffraction limit. Over the past decades, this phenomenon has

offered opportunities for technological advancements in various applications.^{67–69} The recent advent of graphene, along with other emerging 2D materials, has further propelled the fields by providing a new platform for metaoptics that significantly complements traditional metals, dielectrics, and semiconductors. As an atomically thin 2D Dirac semimetal, doped graphene is recognized to support extremely confined plasmons ($\sim 10^6$ smaller than the diffraction limit) in mid- and far-IR and terahertz region, enabling strong light–matter interactions.⁷⁰ The highly confined plasmon polaritons in graphene can be visualized using the technique of scattering-type scanning near-field optical microscope (s-SNOM),^{71,72} in which the photons scattered by an atomic force microscope tip are used as the excitation source to overcome the momentum mismatch between free-space photon and plasmon.⁷³ On the other hand, plasmonic dissipation has been a major obstacle to realizing low-loss graphene plasmonic modes due to the electron–electron scattering in graphene and electron–phonon scattering at the interface between graphene and substrates. While conducting experiments at low temperatures can reduce the intrinsic electron–electron scattering, encapsulating graphene with h-BN is an effective way to reduce the electron–phonon scattering. It has been shown that the propagation length of plasmon polaritons in h-BN encapsulated graphene can be significantly improved compared with the usual case in bare graphene on SiO₂.⁷⁴ Low-temperature s-SNOM measurement down to 60 K has revealed that the lifetime of graphene plasmon can reach up to 1.6 ps, which is larger than the RT value by 1 order of magnitude.⁷⁵

The most exciting feature of graphene lies in its highly tunable conductivity via doping. In contrast to bulk metals, where the substantial density of free electrons nearly shields external electric fields, graphene is a semimetal characterized by its limited density of states. Its 2D nature enables the efficient induction of free electrons or holes through chemical doping or electrical gating.^{76,77} As a result, the optical response of devices based on graphene plasmon polaritons can be actively manipulated in a way that was not possible before.^{78,79} This property of graphene plasmon polaritons makes them ideal candidates to achieve integrated, multifunctional, and compact mid-IR metaoptics, such as tunable IR sources,⁸⁰ modulators,⁸¹ sensors,^{82,83} and photodetectors,^{84,85} to mention a few. For example, Brar et al.⁸⁰ demonstrated that graphene plasmonic resonators can generate blackbody radiation, featuring narrow spectral emission peaks in the mid-IR region [Fig. 5(a)]. In addition, the frequency and intensity of these spectral responses can be actively modulated by applying external electric fields [Fig. 5(b)]. Due to the strongly confined mode volumes, a large Purcell factor of up to 10^7 can be achieved in graphene plasmonic resonators, enabling a much faster thermal emission modulation rate compared with other tuning mechanisms such as using phase-change materials. This also makes it suitable for designing spatial light modulators in the mid-IR. Kim et al.⁸¹ presented a graphene plasmonic device for the effective transmission of light modulation at 1397 cm^{-1} ($7.16\text{ }\mu\text{m}$) with 28.6% efficiency.

Another important application of tunable graphene plasmon polaritons is mid-IR sensing and detection. Rodrigo et al.⁸² demonstrated an electronically tunable graphene plasmonic biosensor for specific label-free detection of protein monolayers, as shown in Fig. 5(c). By gate-tuning graphene Fermi levels, the resonant frequencies of the biosensor are dynamically tuned to selectively probe the protein at different frequencies, allowing the effective extraction of the refractive index of the protein

[Figs. 5(d)–5(f)]. Moreover, the highly confined graphene plasmon enables unprecedented overlap with nanoscale biomolecules, offering stronger light–protein interactions beyond state-of-the-art metallic plasmonic sensors. The ability to enhance the light absorption in the mid-IR by graphene plasmon also makes it suitable for RT IR detection based on the photothermoelectric effect.^{84,85} With careful design of graphene plasmonic resonant structures, the graphene carrier temperature can be manipulated by the plasmonic excitation of Dirac fermions, which can be controlled by gate-tuning the graphene Fermi level. Such specifically designed wavelength-tunable mid-IR photodetectors exhibit outstanding performance at RT, promising a very potential strategy for uncooled, tunable, and multi-spectral IR detection.

While electrostatic gating is very effective in tuning graphene plasmons, the layered structure of graphene also accommodates other possibilities, such as interlayer coupling. Because of interlayer charge tunneling, not only is the plasmon wavelength modified in bilayer graphene but also a turnoff regime for plasmon polaritons in bilayer graphene appears.⁸⁶ Furthermore, in a bilayer graphene with a controlled twist angle of 1.1 deg, chiral and slow plasmon polaritons have been observed.⁸⁷ Interface control of plasmon also applies to heterojunctions between graphene and other 2D materials. For example, in graphene/twisted-WSe₂ heterostructures, the ferroelectric domain of twisted-WSe₂ is imprinted onto the graphene plasmon, forming a domain-like interference pattern when imaged with s-SNOM.⁸⁸ Such a strong interfacial effect implies that graphene plasmon polaritons provide a novel approach to image the electronic structures of interacting layers, for instance, the ferroelectric domain.

Black phosphorus (BP) also supports mid-IR plasmons due to its low carrier density. In contrast to isotropic graphene, BP has a highly anisotropic crystalline structure with highly anisotropic and hyperbolic plasmons that have been studied theoretically.⁸⁹ Despite challenges such as the low air stability and difficulties in large-scale synthesis, tunable and anisotropic mid-IR plasmons have been observed in modified BP grating structures.⁹⁰

Due to their relatively low carrier density ($\sim 10^{17}\text{ m}^{-2}$), graphene and BP are primarily active as highly tunable platforms in the mid- and far-IR range. Fortunately, the diversity of 2D materials makes it feasible to further push tunable plasmon into the near-IR and even visible range. For example, as a boron analog of graphene, borophene (a monolayer boron sheet) is an elemental 2D semimetal that has been theoretically demonstrated to support tunable plasmon polaritons in the near-IR region due to its high density of Dirac electrons ($\sim 10^{19}\text{ m}^{-2}$).⁹³ While there has been no experimental demonstration to date, several device concepts based on tunable borophene plasmon polaritons have been theoretically developed with impressive performance,^{94,95} offering capabilities that are challenging to achieve with other materials. 2D metallic TMDCs such as NbSe₂, NbS₂, and TaSe₂^{91,96,97} can also provide a promising strategy for realizing tunable plasmon polaritons in the near-IR, which has been experimentally demonstrated recently. For example, Zhao et al.⁹¹ reported that NbSe₂ supports electrostatic tunable plasmons in the near-IR region [Figs. 6(a) and 6(b)], showing much tighter light confinement than indium tin oxide (ITO) in this wavelength region [Fig. 6(c)]. By leveraging on the reduced charge screening effect of 2D semimetal and strong gating effect of ionic liquid, NbSe₂ plasmons can be actively tuned within a wide near-IR range, thereby bridging the gap between graphene

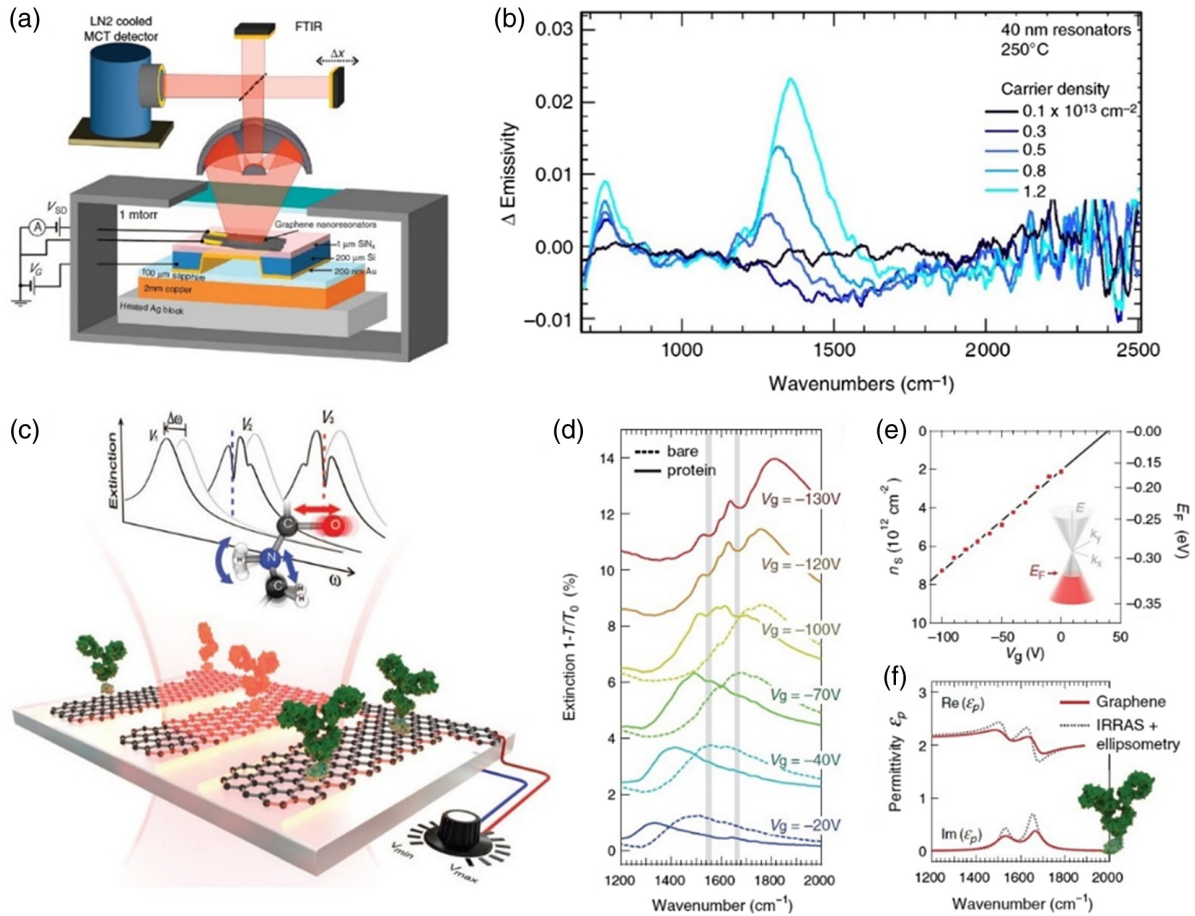


Fig. 5 Tunable graphene plasmon polaritons for mid-IR applications. (a) Schematic of tunable graphene plasmonic resonator for mid-IR radiation. (b) Carrier density dependence of the change in emissivity. (c) Conceptual view of tunable graphene plasmonic biosensor. (d) Extinction spectra of the sensor for bias voltages from -20 to -130 V before (dashed curves) and after (solid curves) protein bilayer formation. (e) Graphene carrier density (n_s) and Fermi energy (E_F) were extracted from experimental IR extinction spectra at different voltages. (f) The permittivity of the protein bilayer extracted from the experimental IR spectra (solid red curves) compared with the permittivity extracted from IR reflection absorption spectroscopy (IRRAS) and ellipsometry measurements (dashed black curves). Panels (a) and (b) were reproduced from Ref. 80 with a CC license, and panels (c)–(f) were reproduced with permission from Ref. 82 © 2015—AAAS.

plasmon and conventional metal/doped semiconductor plasmon [Fig. 6(d)]. Recently, 2D metal carbides and nitrides (MXene) have also been demonstrated to support plasmon polaritons in near-IR regions.^{92,98} Using high-spatial-resolution electron energy-loss spectroscopy (EELS), Guo et al.⁹² characterized the plasmon dispersion of MXene films [Figs. 6(e)–6(h)]. The MXene layer number and momentum are found to have a vital effect on the plasmon-induced electromagnetic absorption.⁹² The vast library of van der Waals 2D materials provides a holistic platform for the realization of tunable plasmon polaritons across the spectral range from visible to mid-far-IR and terahertz, enabling tunable metaoptics that are previously unattainable with conventional plasmonic materials.

3.2 Tunable PhPs

In contrast to plasmon polaritons, PhPs arising from phonon excitation are limited by phonon scattering loss instead of electronic losses. Hence, PhPs have the potential to be low loss with

strong field confinement using crystals with high structural quality. h-BN was the first 2D material in which PhPs were observed. Similarly, using s-SNOM, the real-space imaging of mid-IR PhPs in h-BN has been achieved.³⁹ Compared with graphene plasmons, the PhPs in h-BN show similar field confinement of $\lambda_{IR}/\lambda_p \sim 50$, where λ_{IR} is the incident IR light wavelength and λ_p is the phonon polariton wavelength, but with much longer propagation length up to $10 \mu\text{m}$ than that for graphene plasmon (less than $1 \mu\text{m}$).³⁹ While improving crystal quality is effective in reducing the damping of PhPs, phonon scattering due to interfaces is still limiting the propagation length. To reduce phonon scattering by the substrate, h-BN on monocrystalline gold substrates³⁹ was developed to support PhPs with a propagation length twice as long as h-BN on SiO_2 . Using isotope doping to modify the Reststrahlen band's dispersion, ultralow loss PhPs in isotopic h-BN have been observed, with a threefold improvement in polariton lifetime.¹⁰⁰ Nanopatterning has also been demonstrated to be an effective way to tune h-BN PhPs. For example, ultra-confined resonances

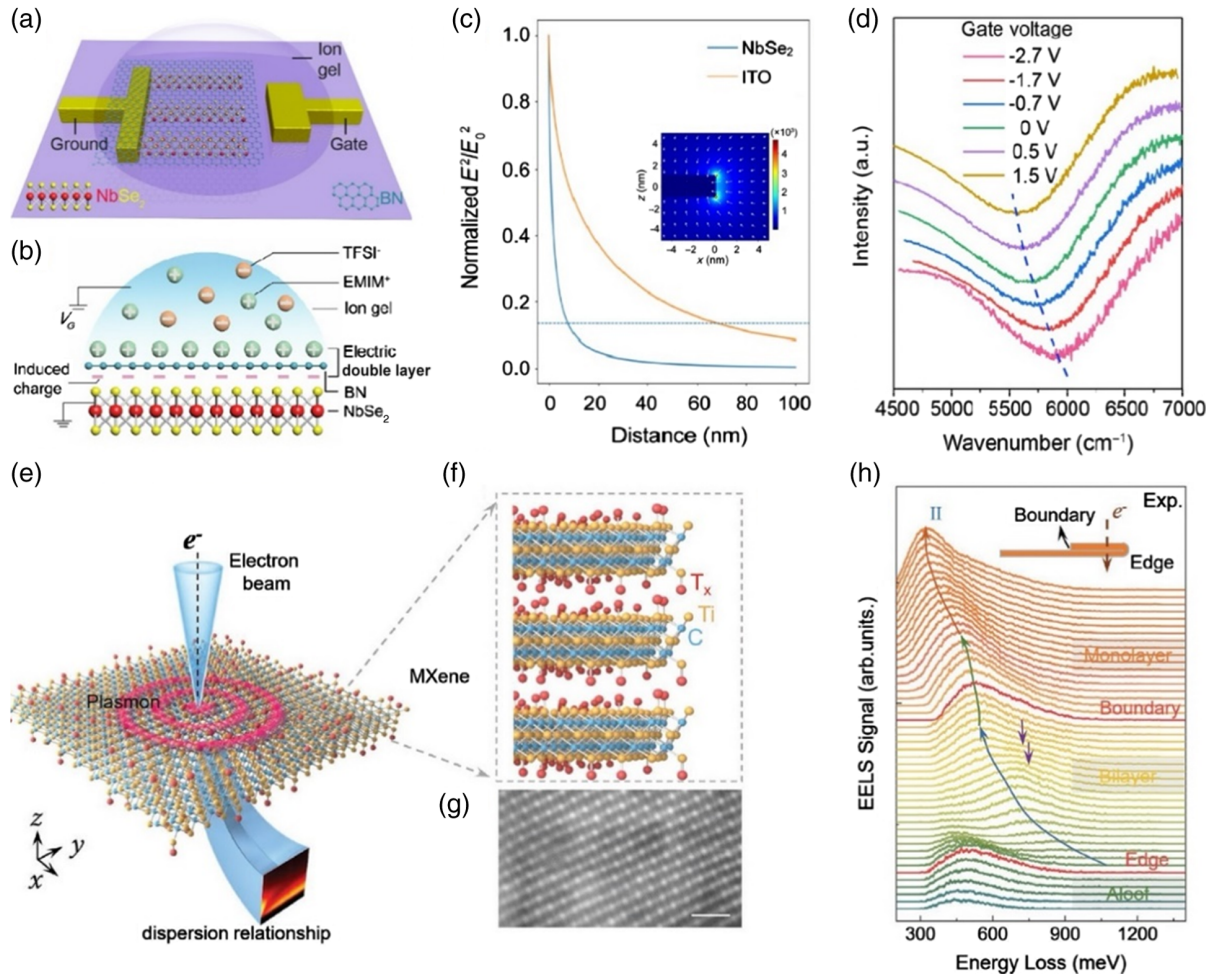


Fig. 6 Tunable 2D plasmon polaritons in near-IR: (a) measurement configurations of tunable NbSe₂ plasmonics, (b) electrostatic-induced gating principle using ion gel. (c) Normalized electric field intensity as a function of the distance from the surface of NbSe₂ and ITO nanoribbons. (d) Tunable plasmonic resonance with varying gate voltage. (e) Schematic diagram of electron-excited MXene plasmon via EELS. (f) Diagram of the lattice structure and the chemical compositions of MXene. (g) High-angle annular dark-field transmission electron microscopy image of MXene film. (h) Experimental EELS spectra in MXene film. Panels (a)–(d) were reproduced with permission from Ref. 91 © 2021—Wiley, and panels (e)–(h) were reproduced with permission from Ref. 92 © 2022—AAAS.

and strong field confinement of PhPs have been demonstrated in h-BN planar nanostructures.¹⁰¹

Although the insulating nature of h-BN makes its PhPs incompatible with electrostatic control such as in graphene and NbSe₂, PhPs in h-BN can be passively tuned with crystal thickness and by tailoring the surrounding dielectric environment, in terms of both phonon polariton intensity and wavelength. Lately, by combining the merits of ultralow-loss phononics and active-tunable graphene plasmonics, Duan et al.¹⁰² observed the active tunable PhPs in the h-BN nanoantenna on top of a graphene layer [Fig. 7(a)]. The near-field image experiences a significant change, and the resonant spectrum exhibits a clear shift as the graphene Fermi level varies, providing concrete proof of an actively tunable h-BN phonon polariton [Figs. 7(b)–7(d)]. The result suggests that combining h-BN nanoantennas with graphene not only reduces ohmic losses in graphene plasmon but also preserves their active tunability, which paves the

way for applications demanding tunable spectral selectivity and strong light–matter interaction.

α -MoO₃ recently has been another material of great interest for phonon polariton research. Real-space imaging has revealed that a mid-IR phonon polariton in α -MoO₃ has comparable field confinement to graphene plasmon but a 10-time longer lifetime.¹⁰⁴ Moreover, a phonon polariton in α -MoO₃ is in-plane anisotropic, with different wavelengths and dispersion along different in-plane crystalline orientations. Topological phase transition has been observed in the phonon polariton of twisted α -MoO₃.^{105,106} As the interlayer twist angle varies, the dispersion contours of phonon polaritons can be altered from hyperbolic to elliptical. The hybridization of phonon polaritons modifies the dispersion lines and, accordingly, the anti-crossing of dispersion lines as well. It has been found that the twist angle-controlled transition is dedicated by a topological quantity, i.e., the number of anti-crossing points of the dispersion relation in reciprocal

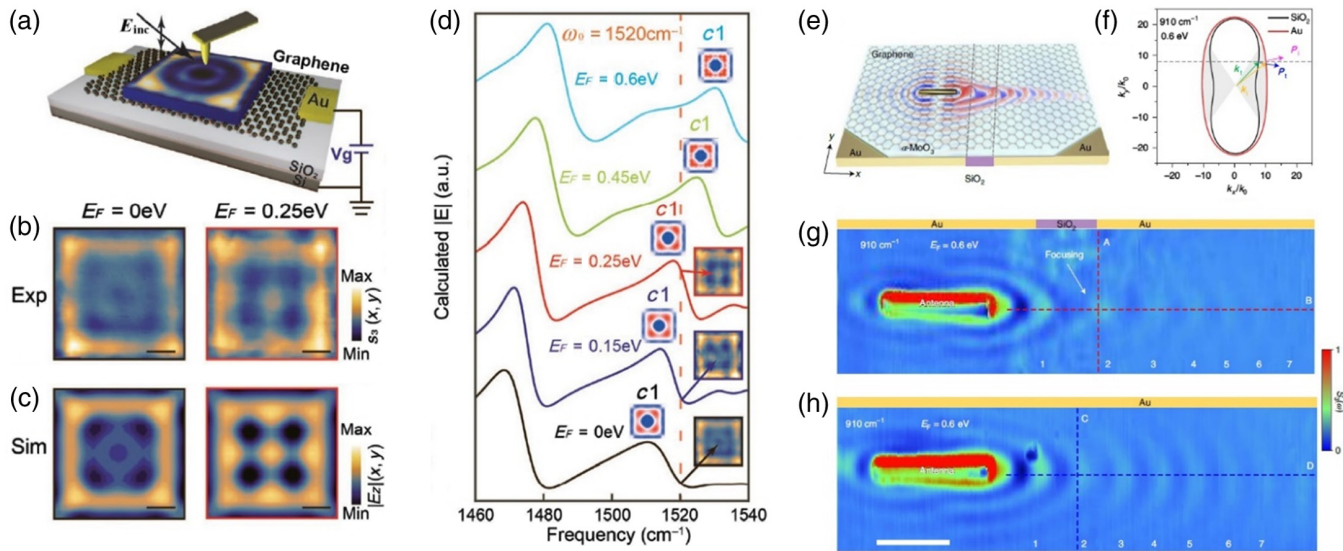


Fig. 7 Tunable PhPs. (a) Schematic of the s-SNOM measurements for gate-tuning PhPs in a square h-BN nanoantenna. (b) Near-field images of PhPs in an h-BN nanoantenna with different graphene Fermi levels. (c) Corresponding calculated images of PhPs. (d) Calculated near-field mid-IR spectra of the h-BN nanoantenna with different graphene Fermi levels. (e) Schematic of the graphene/ α -MoO₃ heterostructure on top of an Au-SiO₂-Au in-plane sandwich substrate. (f) Isofrequency hybrid polaritons dispersion contours for Au and SiO₂ substrates at 910 cm⁻¹. (g) Experimentally measured near-field amplitude image of hybrid polaritons showing partial focusing. (h) Experimentally measured hybrid PhP on a controlled Au substrate. Panels (a)–(d) were reproduced from Ref. 102 with a CC license, and panels (e)–(h) were reproduced from Ref. 103 with a CC license.

space.¹⁰⁵ Similar to the h-BN phonon polariton, the image phonon polariton has also been observed for α -MoO₃ on metal surfaces, with enhanced propagation lifetime due to negligible substrate-mediated loss.¹⁰⁷ In terms of confinement, nanopatterns have been used to improve the quality factor of phonon polariton in α -MoO₃. Specifically, it has been shown that spatially confined freestanding α -MoO₃ on submicrometer-width trenches has a quality factor that is 2 times as high as those on flat substrates.¹⁰⁸ Combining with graphene, it is possible to actively tune the PhPs in α -MoO₃. Recently, Hu et al.¹⁰³ experimentally presented a topological transition in the isofrequency dispersion contours of hybrid polaritons with a graphene/ α -MoO₃ [Fig. 7(e)] heterostructure. By changing the graphene Fermi levels, the contour topology transformed from open to closed shapes over a wide frequency range originating from the doping-dependent polariton hybridization. By further appropriately choosing the substrate, they managed to modify the dispersion contour to achieve improved flatness, which allowed them to realize the subwavelength focusing of polaritons down to 4.8% of the free-space light wavelength through an in-plane lens made of 1.5- μ m-wide silica substrate [Figs. 7(f)–7(h)].

Research in polaritons has made significant progress with the emergence of 2D materials. Regarding the active tuning of polaritons, a highly interesting but so far largely untouched direction is to utilize the rich topological and quantum properties associated with 2D materials as the knob to tune polaritons. The rich physics in 2D polaritonic materials, such as topological states in bilayer graphene,⁶⁸ Ising superconductivity in NbSe₂,⁶⁹ and strong electron correlation in twisted graphene,¹⁰⁹ makes it very appealing to establish connections between polariton excitation and various physics. More interestingly, investigating

different physics in one system is highly viable with 2D materials, and it is possible to open a new playground for polariton studies and applications covering a wide spectral range from the visible to the terahertz.

4 Nonlinear Metaoptics with 2D Materials

4.1 Fundamentals of Nonlinear Metaoptics

Nonlinear metasurfaces have recently emerged as a promising platform to study the nonlinear optical phenomena in a planar system.⁴⁶ Realizing nonlinear phenomena such as wavelength conversion and switching in planar surfaces is important for optical information processing. In the earlier stage of development, plasmonic metasurfaces based on metallic subwavelength structures were employed to explore nonlinear phenomena due to the extreme subwavelength confinement of metallic elements and the possible nonlinear optical response of metals.¹¹⁰ However, the thermal heating and high dissipative losses associated with plasmonic metasurfaces limit their wide application. All-dielectric metasurfaces made of high refractive index materials have been proposed as an alternative for nonlinear metasurface development for their low loss and high damage threshold.⁴³ In addition to electronic nonlinear effects, the optically induced magnetic resonance supported by all-dielectric metasurfaces further enhances the nonlinear optical responses. Besides the well-known nonlinear phenomena such as harmonic generation and parametric frequency conversion, all-dielectric nonlinear metasurfaces can also be used to realize other interesting nonlinear functionalities using the underlying physics of Mie resonances⁴ and the collective resonance such as guided-mode

resonance and optical bound states in the continuum (BICs).¹¹¹ The new functionalities introduced by nonlinear metasurfaces include^{45,112} asymmetric and chiral frequency conversion, multi-frequency and cascading effects, nonlinear quantum photonics, and nonperturbative nonlinear regimes.

The second- and third-order nonlinear processes such as second-harmonic generation (SHG) and third-harmonic generation (THG), respectively, are the most common nonlinear optical effects. Even though these nonlinear effects are phase-sensitive, the required phase-matching condition is not necessary in the metasurface due to its subwavelength scale dimension.¹¹² In particular, the light interaction happens at a subwavelength scale much smaller than the coherence length of the light. To realize an efficient nonlinear metasurface, it requires:⁴⁵ (i) high nonlinear susceptibility value, (ii) large electromagnetic field enhancement at the resonances of metasurface and overlap of these resonances with fundamental and newly generated wave frequencies, and (iii) low loss of material at both the fundamental and newly generated wave frequencies. The field enhancement is due to Mie-type resonance such as electric and magnetic dipole resonances, and anapole resonance at the fundamental frequency has been widely employed to boost the nonlinear process in all-dielectric metasurfaces.^{45,111,112} In addition, high-quality factor BIC resonance realized in some metasurfaces can further enhance the nonlinear effects due to exceptionally high electromagnetic field enhancement at the fundamental frequency.⁴⁵

4.2 Nonlinear Optical Properties of 2D Materials

In recent years, 2D materials and their hybrid structures have shown their great potential for nonlinear optics.⁴⁶ The first 2D material, graphene, exhibits a wide spectrum of nonlinear optical properties such as saturable absorption (SA),¹¹³ THG,¹¹⁴ four-wave mixing (FWM),¹¹⁵ self-phase modulation,¹¹⁶ coherent optical injection,¹¹⁷ optical limiting,¹¹⁸ and nonlinear Kerr effect.¹¹⁹ A second-order nonlinear process such as SHG is not possible in graphene due to its centrosymmetric crystal structure. However, SHG has been realized at the interface of graphene/SiO₂/Si systems by breaking the inversion symmetry.^{120,121} Various physical and chemical methods have also been proposed for breaking the inversion symmetry.^{47,109,110} The ability to tune the linear and nonlinear optical properties of graphene shows the key role of graphene in future reconfigurable optoelectronic devices.

TMDCs including MoS₂, MoSe₂, WS₂, and WSe₂ exhibit indirect-to-direct bandgap transition as their thickness is reduced from the bulk to the monolayer form and have shown fascinating linear and nonlinear optical properties. Using both monolayer and few-layer TMDCs, nonlinear effects have been demonstrated, including SA,¹²² SHG,¹²³ THG,¹²⁴ sum-and-difference frequency generation,¹²⁵ higher-harmonic generation (HHG),¹²⁶ optical limiting,¹²⁷ and FWM.¹²⁸ In contrast to graphene, second-order and other even-order nonlinear processes can happen in TMDCs because they do not have inversion symmetry with an odd number of layers. The monolayer TMDC can provide large second-order nonlinear susceptibilities in the range of 1 to 10⁵ pm/V, and the enhancement of SHG is due to the overlap of the C-exciton resonance of TMDCs with the SHG wavelength.¹¹² This interesting feature is also useful for spintronic and valleytronic applications.¹²⁹

Many other 2D materials have also exhibited interesting nonlinear optical properties. Compared with graphene and TMDCs,

BP has been reported of significantly higher bandgap tunability of ~0.3 to ~2.0 eV through crystal thickness manipulation.¹³⁰ In addition, BP is a suitable material for anisotropic optics because it has an anisotropic crystal structure. The nonlinear susceptibility of BP is high at ~10⁻¹⁹ m² V⁻² and has been utilized to realize THG,¹³¹ FWM,¹³² and SAs.¹³³ However, the stability of BP is a limiting factor and proper encapsulation, or other methods are required to protect BP for long-term stability.¹³⁴ Moreover, other systems such as h-BN¹³⁵ and groups III and IV metal chalcogenides (GeSe and SnS)¹³⁶ have received wide interest. In Table 1, we summarize the nonlinear optical responses of different 2D materials.⁴⁶

The hybrid structures of 2D materials are currently receiving significant attention to engineer their linear and nonlinear optical properties, where each 2D material layer can be smartly designed to control the desired functions independently.¹³⁷ With the advent of advanced growth and fabrication methods, the heterostructures of 2D materials can easily be fabricated by stacking different 2D materials. To date, various 2D material combinations, including graphene-h-BN, -BP, TMDC-BN, -BP, -graphene, and TMDC-TMDC have been utilized to realize 2D heterostructures for numerous photonics applications.⁴⁹ In these structures, the nonlinear effects can be enhanced by the coherent superposition of the optical fields from the individual layers. So far, nonlinear effects such as SHG¹³⁸ and SA¹³⁹ have been demonstrated using 2D heterostructures. The design of a proper heterostructure superlattice is required to explore the other higher-order nonlinear effects.

4.3 Nonlinear Metasurfaces Based on 2D Materials

Metasurfaces based on 2D materials have the advantages of a high refractive index, ultrathin thickness, tunable features, high-*Q* resonance, and enhanced nonlinear response.¹⁴⁰⁻¹⁴⁷ Significant nonlinear effects were observed in 2D metasurfaces compared with monolayer and few-layers of 2D materials alone. Popkova et al.¹⁴¹ reported nonlinear exciton-Mie resonance coupling and second-order nonlinear effects using bulk MoS₂. As shown in Figs. 8(a)–8(d), nanodisks were fabricated on a thick flake of MoS₂ and achieved 23-fold enhancement of SHG compared with an unpatterned monolayer of MoS₂ for a fundamental wavelength of 900 nm. Here, the metasurface was carefully designed to excite the Mie-type resonance at 900 nm wavelength and to overlap the second-harmonic wavelength at C-exciton resonance of MoS₂ (450 nm), and as a result, a huge field enhancement was achieved at both the fundamental and newly generated wave frequencies. The observed enhanced SHG is also due to the anisotropic nature of fabricated nanodisks, which originated from the hexagonal crystalline structure.

A similar kind of result was reported by Panmai et al.,¹⁴² where the authors fabricated hexagonal-prism-like nanostructures in a thick flake of MoS₂. The Mie resonance was excited at the near-IR wavelengths, and the second-harmonic wave was generated around the C-exciton resonance of MoS₂ [Figs. 8(e) and 8(f)]. The authors also discussed the importance of the mode profile to enhance the nonlinear optical effects in TMDC metasurfaces, as they observed enhanced and suppressed SHG at electric dipole and electric quadrupole resonance, respectively. In a very recent paper,¹⁴³ authors reported >100-fold enhancement of SHG from a single MoS₂ nanodisk patterned on a 3R phase MoS₂ multilayer [Figs. 8(g) and 8(h)]. Note that the patterned 3R-MoS₂ nanodisk excites nonradiating Mie

Table 1 2D materials and their nonlinear optical responses.

2D material	Nonlinear effect ^a	Nonlinear coefficient ^b	Emission wavelength (nm) ^c	Thickness ^d
Graphene	THG	42,000	263 to 1030	ML
	FWM	14,000	360 to 1566	ML; FL
MoS ₂	SHG	10,000	370 to 780	ML; BL; FL
	THG	2.4	520 to 660	ML
	FWM	—	430 to 450	FL
MoSe ₂	SHG	5	600 to 900	ML
	THG	2.2	520	ML
	FWM	—	750	ML
WS ₂	SHG	900	415 to 660	ML
	THG	2.4	520	ML
WSe ₂	SHG	1000	400 to 795	ML; BL
	THG	1	520	ML
GaSe	SHG	240	400 to 800	ML; FL
	THG	1600	520	FL
GaTe	SHG	0.115	760	7 to 57 nm
	THG	2000	520	7 to 57 nm
BP	THG	1.6	520	10 nm; 1L to 4L
	FWM	—	1550	4.3 nm; 18 nm
MoTe ₂	SHG	5	500	FL
ReS ₂	THG	53	505	ML
InSe	SHG	—	530	9 to 25 nm
hBN	SHG	200	405	ML; BL; FL

^aThe most common nonlinear effects are highlighted.

^bMaximum achieved values of the nonlinear coefficient are reported, for SHG, $\chi^{(2)} \times 10^{-11}$ m/V; for THG and FWM, $\chi^{(3)} \times 10^{-19}$ m²/V².

^cThe spectral ranges of newly generated waves for SHG, THG, and FWM are reported.

^dThickness of 2D materials, ML, monolayer; BL, bilayer; and FL, few-layer.

resonance such as anapole resonance, and the reported >100-fold enhancement is obtained by comparing it with an unpatterned MoS₂ multilayer. The anapole resonance and MoS₂ disk were further employed to realize enhanced third-order nonlinear effects such as FWM.¹⁴⁴ Compared with unpatterned MoS₂ flakes, an enhancement factor of 150 times at 1470 nm pump wavelength was realized using a 3R-MoS₂ disk with a diameter and thickness of 1.62 μ m and 108 nm, respectively.

Even though the nonlinear metasurfaces operate at a subdiffraction regime for the fundamental wave, the emission of multiple diffractive beams at the nonlinearly generated harmonics restricts directional emission from such metasurfaces. This issue was addressed in a recent paper by Nauman et al.,¹⁴⁵ in which the authors used a Mie-resonant metasurface made up of truncated cones of MoS₂ [Figs. 9(a)–9(c)]. By exploiting the extremely high refractive index of MoS₂, the unidirectional emission of SHG and THG with tunable SHG emission in forward and backward directions was realized [Figs. 9(d) and 9(e)]. Along the same direction, Shi et al.¹⁴⁶ proposed a Fabry–Perot microcavity-coupled monolayer WS₂ platform for direction and enhanced SHG [Figs. 9(f) and 9(g)]. The strong electric field enhancement at the resonance of the microcavity benefited the enhanced and directional emission of SHG (diverging angle of ~ 5 deg). Du et al.¹⁴⁷ also demonstrated directional SHG

emission using a heterostructure of MoS₂/WS₂ monolayer, which was suspended on a holey SiO₂/Si substrate.

The aforementioned nonlinear metasurfaces have mainly been used to investigate the common nonlinear optical effects such as SHG and THG through exploiting the physics of Mie resonance. However, the excitation of high-*Q* resonances at the fundamental wave frequencies is important to further improve the efficiency of second- and third-order nonlinear effects and to generate higher-order nonlinear processes. Kühner et al.¹⁴⁸ experimentally demonstrated high-*Q* resonance such as quasi-BIC using h-BN metasurfaces. Although h-BN is a low refractive index dielectric, the authors showcased symmetry-broken quasi-BIC resonance with a *Q*-factor of >300 over a spectral band from 400 to 1000 nm by fabricating the slit array metasurface on a single h-BN flake [Figs. 10(a) and 10(b)]. By utilizing the enhanced electric near-field distribution at the quasi-BIC resonance, a 388-fold second-harmonic enhancement factor in the ultraviolet wavelength band was reported [Fig. 10(c)].¹⁴⁸ There are also a few experimental reports on the realization of quasi-BIC resonance by integrating TMDCs with all-dielectric metasurfaces for boosting the second-order nonlinear processes.^{149–152}

Since the main challenges associated with nonlinear optics in all-dielectric metasurfaces at the shorter wavelengths (visible

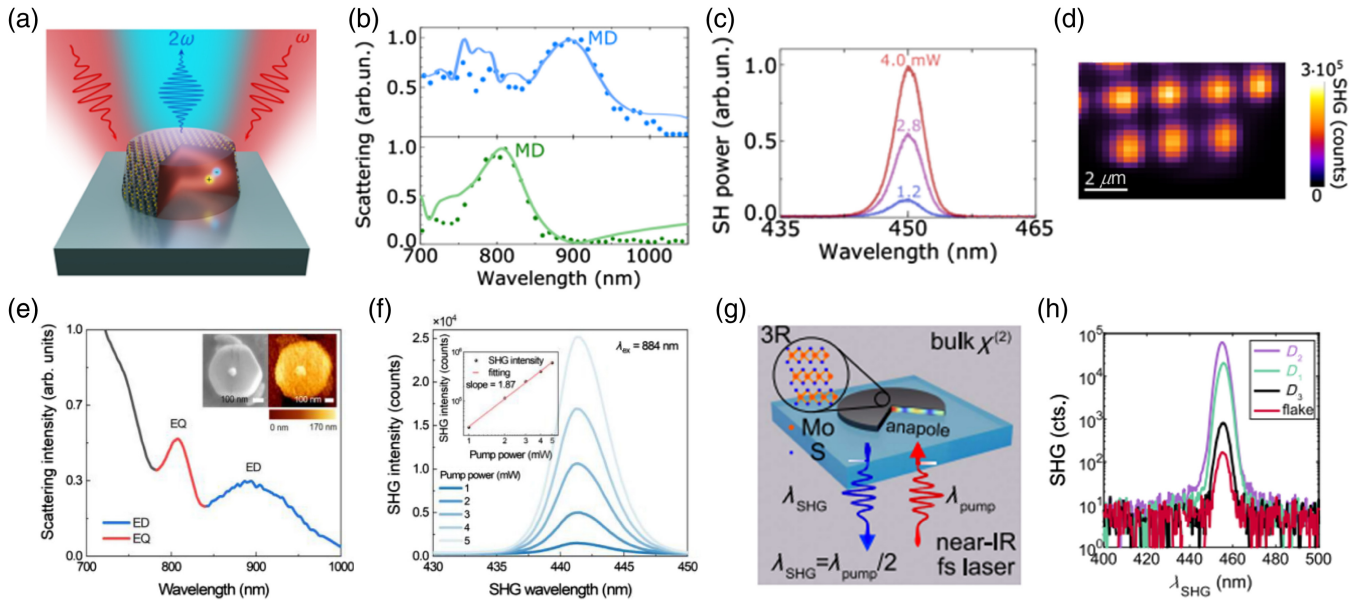


Fig. 8 SHG from MoS₂. (a) Schematic representation of the SHG using MoS₂ nanodisks. (b) Measured (dot) and calculated (curve) scattering spectra of MoS₂ nanodisk metasurface for different disk diameters (550 nm for blue and 300 nm for green). (c) Measured second-harmonic signal from a single nanodisk for different pump powers. (d) Mapping of second-harmonic intensity over the nanodisk array at a pump wavelength of 900 nm. (e) Measured scattering spectrum from a MoS₂ nanoparticle. (f) Measured second-harmonic signal from a MoS₂ nanoparticle shown in the inset of panel (e) for different pump powers at a wavelength of 884 nm. (g) Schematic representation of the SHG in 3R-MoS₂ nanodisks. (h) Measured second-harmonic spectrum of 3R-MoS₂ nanodisks with different disk diameters at a pump wavelength of 910 nm. Panels (a)–(d) were reproduced with permission from Ref. 141 © 2022—Wiley, panels (e) and (f) were reproduced with permission from Ref. 142 © 2023—Wiley, and panels (g) and (h) were reproduced from Ref. 143 with CC license.

and near-IR) are the relatively low refractive index, large mode volumes, and low nonlinear response, the development of novel 2D materials-based nonlinear metasurfaces using the existing advanced techniques of growth, fabrication, and nanopatterning will have a significant impact in this field. Another important aspect of 2D materials is the high tunability of all 2D- and hybrid 2D-material-based nonlinear metasurfaces, as it would allow the efficient spatial and temporal control of light for diverse nonlinear applications. In addition, the tunability feature enables us to realize nonlinear metasurfaces with full all-optical control over the transient behavior of nonlinear response at a possible switching speed of femtoseconds,¹³¹ which is useful for next-generation high-speed data processing. We expect continued interest in this direction to realize other interesting nonlinear effects such as nonlinear quantum photonics, multi-frequency effects, cascaded harmonic generation, and asymmetric frequency conversion. The recently demonstrated concept of Mie voids,¹⁵³ which has the low-index voids surrounded by high-index dielectric and thus has light confined in the voids by localized mode, provides another avenue for the realization of novel 2D material-based resonant metasurfaces with exceptionally high nonlinearities at the nanoscale for the shorter wavelengths.

5 Discussion

From the practical application point of view, 2D-material-based tunable metasurfaces can be used to develop ultrasensitive label-free biosensors,⁷⁹ ultrathin metalenses^{24,154–156} and meta-

holograms,^{157,158} and ultrathin and integrable light sources.¹⁵⁴ In particular, the electrically tunable plasmonic resonance of graphene in the IR wavelength band can be used for IR spectroscopy to identify the vibrational fingerprints of different biomolecules.⁷⁹ Using the tunable feature of the sensor, multiplexed detection is possible by dynamically tuning the spectral positions of the graphene plasmons in a wide spectral band. In addition, flexible photonic devices can also be developed with 2D materials, since they can be easily transferred to flexible materials and substrates, where strain-induced tuning can also be considered as an alternative tuning mechanism.

However, 2D materials still face the issue of stability in practical application. Compared with conventional bulk materials, many 2D materials exhibit susceptibility to the ambient environment.¹⁵⁹ Typically, the degradation arises from their intrinsic instability and atomic-level defects induced by external factors such as oxygen and water adsorption and light illumination.^{160–162} Encapsulation is the primary strategy to stabilize 2D materials.¹⁶³ One way is using a protective layer, such as hBN,^{164,165} atomic layer-deposited high-*k* dielectrics,^{166,167} or polymer capping^{168,169} to isolate 2D materials from the environment directly. The other way is functionalizing 2D materials with organic or inorganic substances to make their surface inert.^{170,171} These two ways can also be combined to further ensure the stability of 2D material-based devices.

Furthermore, a careful selection of 2D material preparation techniques is required to optimize metaoptic performance.

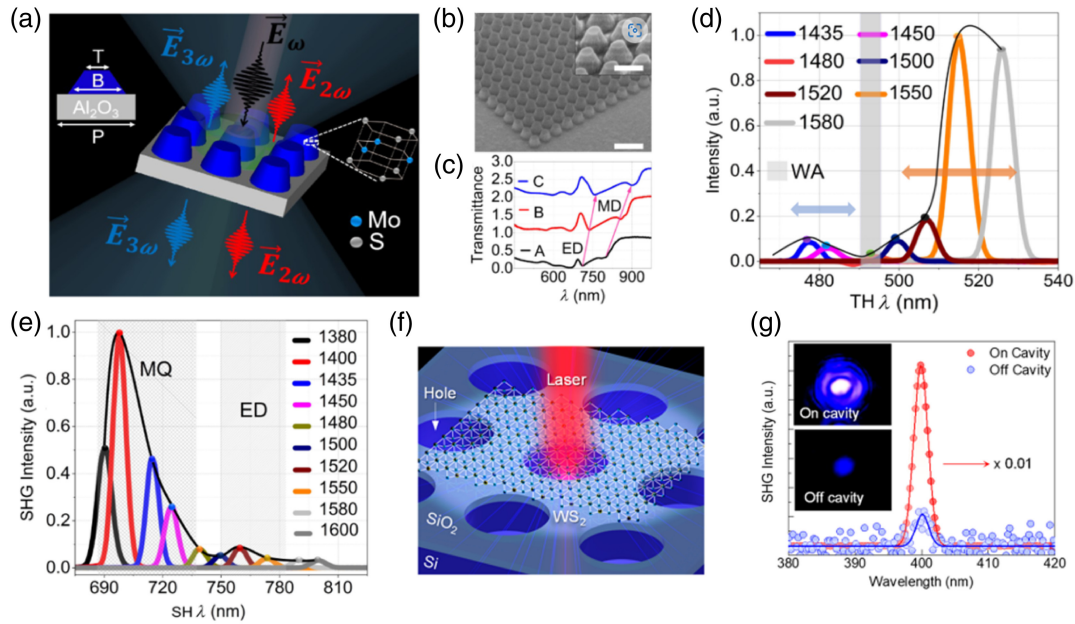


Fig. 9 HHG from TMD metasurfaces. (a) Concept of unidirectional SHG and THG using MoS₂ truncated cone metasurface. (b) Scanning electron microscope (SEM) image of the fabricated metasurface. (c) Measured transmission spectra of metasurface with different structural parameters. Measured wavelength-dependent generation of (d) THG and (e) SHG from the metasurface. (f) Schematic of WS₂ monolayer on a Fabry-Pérot (F-P) microcavity. (g) Measured second-harmonic intensity from the on and off cavity at an excitation wavelength of 800 nm. Panels (a)–(e) were reproduced from Ref. 145 under CC license, and panels (f) and (g) were reproduced with permission from Ref. 146 © 2022—ACS.

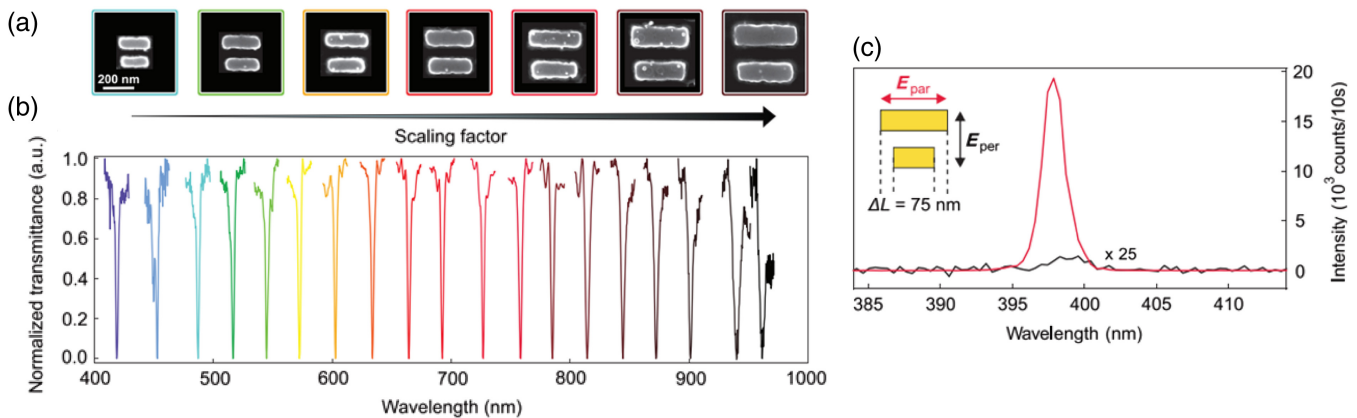


Fig. 10 Quasi-BIC h-BN metasurface. (a) SEM images of the fabricated metasurface unit cell on h-BN with an increasing scaling factor and (b) the corresponding excited high-Q quasi-BIC resonance from 400 to 1000 nm with an increasing scaling factor. (c) Measured second-harmonic signal from quasi-BIC metasurface. This figure is reproduced with permission from Ref. 148 © 2023—Wiley.

Direct synthesis, also known as the bottom-up method, such as the chemical vapor deposition, allows controlled growth of 2D materials on substrates, offering large-area growth,¹⁷² high scalability, and precise control over layer thickness¹⁷³ but simultaneously facing the shortcoming of being substrate-sensitive and requiring high temperature.¹⁷⁴ On the other hand, exfoliation from bulk crystals, also known as the top-down method, promises high-quality flakes, with the drawback of miniature flake sizes.^{175–177} This technique includes mechanical exfoliation,

liquid-phase exfoliation, and more recently, electrochemical exfoliation. A summary of the key features of the exfoliation methods is presented in Table 2a. Moreover, in producing tunable metaoptics, it is noteworthy that nanopatterning of 2D materials is a crucial technique,^{183,184} with the top-down approach being the primary method. Various common top-down approaches, ranking from the highest to the lowest in patterning resolution, include lithography and etching,^{24,37,61,62} tip or ion-assisted direct patterning,^{22,26} and optical direct-patterning,²³

Table 2 2D materials preparation methods. We summarize the key features of the common top-down approaches in 2D materials preparation for (a) exfoliation and (b) nano-patterning.

Method	Typical size	Key features	Pros	Cons	Ref.
(a)					
Mechanical exfoliation	nm to μm	Use adhesive tapes to delaminate bulk materials, ideal for research	High-quality flakes, preserving material intrinsic properties	Limited scalability, being labor intensive, and miniature flake sizes	175–177
Liquid-phase exfoliation	nm to μm	Use adhesive tapes to delaminate bulk materials, ideal for scalable production	High versatility and scalability	Reduced flake quality from solvent residue	178–180
Electrochemical exfoliation	Up to hundreds of μm	Use electric fields to exfoliate materials either in solution or on electrodes, ideal for device fabrication	Large size samples, high scalability and tunability, limited environmental impact	Limited throughput	91, 181, and 182
(b)					
Lithography (UV and DUV, e-beam) and etching	From μm to 10 nm	Pattern creation via lithography and etching, can achieve high resolution and integration	Being compatible with existing semiconductor processes; high precision	Potential damage from etching processes; photoresist residues	24, 37, 61, and 62
Tip or ion-assisted direct patterning	Sub-100 nm	Direct pattern writing with tip or ion offers customization and clean surfaces	Avoiding photoresist residues; enabling customized patterning	Generally slower process; higher cost for high-resolution patterns	22 and 26
Optical direct patterning	Down to 100 nm	Direct pattern writing by high-power laser offers customization and clean surfaces	Avoiding photoresist residues; enabling customized patterning	Lower resolution compared with the other two methods	23

all bearing their respective merits and drawbacks that warrant deliberate consideration for performance optimization. A list of the common techniques discussed in this review is summarized in Table 2b.

6 Conclusion

In this review, we focused on the current rising research interest in tunable 2D material-based metaoptics to provide a detailed coverage of the progress, challenges, and prospects of this area. We introduced the channels to enable tunability in 2D systems, including excitons, trions, plasmon, and PhPs and then discussed the recent advancements in the nonlinear metaoptics made of 2D materials.

First, we highlighted the promises of excitons and trions as the knobs to achieve the tunability of metaoptics. We showcased the uniqueness of these quasi-particles in the 2D system and discussed how their strong and controllable resonances enable state-of-the-art 2D material-based tunable metaoptics. The specific challenges faced in this direction and the needs to be addressed by the community are also assessed like uniform electrostatic gating across a large 2D sample in the future and broadband excitonic tunability.

Second, 2D polaritons are discussed, which offer another avenue to enable large tunability 2D metaoptics with strong light–matter interaction. 2D plasmon polaritons in semimetals cover a wide spectral range from far- to near-IR, while 2D PhPs in both h-BN and α -MoO₃ have a significantly longer lifetime and the potential to improve the quality factor of the metaoptics, which could see more applications such as in nonlinear optics and quantum photonics. s-SNOM is particularly a powerful tool in direct visualization and manipulation of polaritons in 2D metaoptics. Further understanding of the nontrivial tip–sample interaction and spatial-temporal s-SNOM measurement would greatly benefit the 2D metaoptics and 2D materials study in general.

Finally, we presented the 2D nonlinear metaoptics in which 2D materials and their hybrid structures are used either as the nonlinear media or metaoptics themselves. Various nonlinear effects, including SHG and HHG with good efficiency and high-quality factors, have been demonstrated to address the shortcomings of all-dielectric metasurfaces. The tunable nonlinear metasurfaces using all-2D materials are yet to emerge and would be an interesting direction to explore.

The unique properties possessed by various 2D materials, such as high refractive index, tunable excitons, and polariton resonance by gate voltage, forming moiré superlattices, strong interlayer coupling, a van der Waals nature for easy integration with various substrates and constructing heterostructures, rich choices of materials in semiconductor, semimetal, ferroelectric, ferromagnetic, and large nonlinear coefficients, make the 2D system a promising platform for tunable and nonlinear metaoptics. Further fundamental studies of physics and materials and technological advancements in material growth, stacking, and nanofabrication would unleash the full potential of 2D tunable and nonlinear metaoptics to benefit photonics-in-general development.

Disclosures

The authors declare no competing financial interests.

Code and Data Availability

Data sharing is not applicable to this article as no datasets were generated or analyzed during the current study.

Acknowledgments

This work is financially supported by the National Research Foundation Singapore under CRP program (Grant No. NRF-CRP26-2021-0004), the Agency for Science, Technology, and Research (A*STAR) under the AME IRG Program (Grant Nos. A2083c0058 and A20E5c0084), the MTC Program (Grant No. M22L1b0110), and the HBMS IAF-PP (Grant No. H19H6a0025).

References

1. D. R. Smith, J. B. Pendry, and M. C. K. Wiltshire, “Metamaterials and negative refractive index,” *Science* **305**, 788–792 (2004).
2. I. Staude and J. Schilling, “Metamaterial-inspired silicon nanophotonics,” *Nat. Photonics* **11**, 274–284 (2017).
3. S. Jahani and Z. Jacob, “All-dielectric metamaterials,” *Nat. Nanotechnol.* **11**, 23–36 (2016).
4. N. Yu and F. Capasso, “Flat optics with designer metasurfaces,” *Nat. Mater.* **13**, 139–150 (2014).
5. A. M. Shaltout, V. M. Shalae, and M. L. Brongersma, “Spatiotemporal light control with active metasurfaces,” *Science* **364**, eaat3100 (2019).
6. J. Park et al., “All-solid-state spatial light modulator with independent phase and amplitude control for three-dimensional LiDAR applications,” *Nat. Nanotechnol.* **16**, 69–76 (2021).
7. V. E. Babicheva, A. Boltasseva, and A. V. Lavrinenko, “Transparent conducting oxides for electro-optical plasmonic modulators,” *Nanophotonics* **4**, 165–185 (2015).
8. Z. Wang et al., “A novel chiral metasurface with controllable circular dichroism induced by coupling localized and propagating modes,” *Adv. Opt. Mater.* **4**, 883–888 (2016).
9. C. Enkrich et al., “Magnetic metamaterials at telecommunication and visible frequencies,” *Phys. Rev. Lett.* **95**, 203901 (2005).
10. Q. Zhao et al., “Mie resonance-based dielectric metamaterials,” *Mater. Today* **12**, 60–69 (2009).
11. A. Nemati et al., “Tunable and reconfigurable metasurfaces and metadevices,” *Opto-Electron. Adv.* **1**, 18000901 (2018).
12. O. A. M. Abdelraouf et al., “Recent advances in tunable metasurfaces: materials, design, and applications,” *ACS Nano* **16**, 13339–13369 (2022).
13. O. Buchnev et al., “Electrically controlled nanostructured metasurface loaded with liquid crystal: toward multifunctional photonic switch,” *Adv. Opt. Mater.* **3**, 674–679 (2015).
14. T. Badloe et al., “Liquid crystal-powered Mie resonators for electrically tunable photorealistic color gradients and dark blacks,” *Light Sci. Appl.* **11**, 118 (2022).
15. S.-Q. Li et al., “Phase-only transmissive spatial light modulator based on tunable dielectric metasurface,” *Science* **364**, 1087–1090 (2019).
16. C. Zheng et al., “Enabling active nanotechnologies by phase transition: from electronics, photonics to thermotics,” *Chem. Rev.* **122**, 15450–15500 (2022).
17. S. Lepeshov and A. Krasnok, “Tunable phase-change metasurfaces,” *Nat. Nanotechnol.* **16**, 615–616 (2021).
18. Y. Zhang et al., “Electrically reconfigurable non-volatile metasurface using low-loss optical phase-change material,” *Nat. Nanotechnol.* **16**, 661–666 (2021).
19. Y. Wang et al., “Electrical tuning of phase-change antennas and metasurfaces,” *Nat. Nanotechnol.* **16**, 667–672 (2021).
20. G. Wang et al., “Colloquium: excitons in atomically thin transition metal dichalcogenides,” *Rev. Mod. Phys.* **90**, 021001 (2018).

21. R. Mas-Ballesté et al., “2D materials: to graphene and beyond,” *Nanoscale* **3**, 20–30 (2011).
22. Z. Wang et al., “Exciton-enabled meta-optics in two-dimensional transition metal dichalcogenides,” *Nano Lett.* **20**, 7964–7972 (2020).
23. Y. Wang et al., “Atomically thin noble metal dichalcogenides for phase-regulated meta-optics,” *Nano Lett.* **20**, 7811–7818 (2020).
24. C.-H. Liu et al., “Ultrathin van der Waals metalenses,” *Nano Lett.* **18**, 6961–6966 (2018).
25. A. Rodin et al., “Collective excitations in 2D materials,” *Nat. Rev. Phys.* **2**, 524–537 (2020).
26. A. Dasgupta, J. Gao, and X. Yang, “Atomically thin nonlinear transition metal dichalcogenide holograms,” *Nano Lett.* **19**, 6511–6516 (2019).
27. Y. Yu et al., “Giant gating tunability of optical refractive index in transition metal dichalcogenide monolayers,” *Nano Lett.* **17**, 3613–3618 (2017).
28. M. Li et al., “Refractive index modulation in monolayer molybdenum diselenide,” *Nano Lett.* **21**, 7602–7608 (2021).
29. K. F. Mak et al., “Tightly bound trions in monolayer MoS₂,” *Nat. Mater.* **12**, 207–211 (2013).
30. P. Chen et al., “Approaching the intrinsic exciton physics limit in two-dimensional semiconductor diodes,” *Nature* **599**, 404–410 (2021).
31. D.-H. Lien et al., “Electrical suppression of all nonradiative recombination pathways in monolayer semiconductors,” *Science* **364**, 468–471 (2019).
32. M. G. Harats et al., “Dynamics and efficient conversion of excitons to trions in non-uniformly strained monolayer WS₂,” *Nat. Photonics* **14**, 324–329 (2020).
33. J. S. Ross et al., “Electrical control of neutral and charged excitons in a monolayer semiconductor,” *Nat. Commun.* **4**, 1474 (2013).
34. Q. Zhang et al., “Simultaneous capturing phonon and electron dynamics in MXenes,” *Nat. Commun.* **13**, 7900 (2022).
35. A. N. Grigorenko, M. Polini, and K. S. Novoselov, “Graphene plasmonics,” *Nat. Photonics* **6**, 749–758 (2012).
36. M. Sebek et al., “Hybrid plasmonics and two-dimensional materials: theory and applications,” *J. Mol. Eng. Mater.* **8**, 2030001 (2020).
37. P. Li et al., “Infrared hyperbolic metasurface based on nanostructured van der Waals materials,” *Science* **359**, 892–896 (2018).
38. A. Elbanna et al., “2D material infrared photonics and plasmonics,” *ACS Nano* **17**, 4134–4179 (2023).
39. S. Dai et al., “Tunable phonon polaritons in atomically thin van der Waals crystals of boron nitride,” *Science* **343**, 1125–1129 (2014).
40. A. Krasnok, M. Tymchenko, and A. Alù, “Nonlinear metasurfaces: a paradigm shift in nonlinear optics,” *Mater. Today* **21**, 8–21 (2018).
41. T. Huang et al., “Planar nonlinear metasurface optics and their applications,” *Rep. Prog. Phys.* **83**, 126101 (2020).
42. E. Rahimi and R. Gordon, “Nonlinear plasmonic metasurfaces,” *Adv. Opt. Mater.* **6**, 1800274 (2018).
43. B. Sain, C. Meier, and T. Zentgraf, “Nonlinear optics in all-dielectric nanoantennas and metasurfaces: a review,” *Adv. Photonics* **1**, 024002 (2019).
44. G. Grinblat, “Nonlinear dielectric nanoantennas and metasurfaces: frequency conversion and wavefront control,” *ACS Photonics* **8**, 3406–3432 (2021).
45. T. Pertsch and Y. Kivshar, “Nonlinear optics with resonant metasurfaces,” *MRS Bull.* **45**, 210–220 (2020).
46. A. Autere et al., “Nonlinear optics with 2D layered materials,” *Adv. Mater.* **30**, 1705963 (2018).
47. T. Jiang et al., “Gate-tunable third-order nonlinear optical response of massless Dirac fermions in graphene,” *Nat. Photonics* **12**, 430–436 (2018).
48. B. Huang et al., “Tuning inelastic light scattering via symmetry control in the two-dimensional magnet CrI₃,” *Nat. Nanotechnol.* **15**, 212–216 (2020).
49. Z. Sun, A. Martinez, and F. Wang, “Optical modulators with 2D layered materials,” *Nat. Photonics* **10**, 227–238 (2016).
50. G. Wang et al., “Giant enhancement of the optical second-harmonic emission of WSe₂ monolayers by laser excitation at exciton resonances,” *Phys. Rev. Lett.* **114**, 097403 (2015).
51. A. Chernikov et al., “Exciton binding energy and nonhydrogenic Rydberg series in monolayer WS₂,” *Phys. Rev. Lett.* **113**, 076802 (2014).
52. J. Lynch et al., “Exciton resonances for atomically-thin optics,” *J. Appl. Phys.* **132**, 091102 (2022).
53. M.-J. Lee et al., “Measurement of exciton and trion energies in multistacked hBN/WS₂ coupled quantum wells for resonant tunneling diodes,” *ACS Nano* **14**, 16114–16121 (2020).
54. T. Goldstein et al., “Ground and excited state exciton polarons in monolayer MoSe₂,” *J. Chem. Phys.* **153**, 071101 (2020).
55. K. Wagner et al., “Autoionization and dressing of excited excitons by free carriers in monolayer WSe₂,” *Phys. Rev. Lett.* **125**, 267401 (2020).
56. A. Arora et al., “Excited-state trions in monolayer WS₂,” *Phys. Rev. Lett.* **123**, 167401 (2019).
57. A. Chernikov et al., “Electrical tuning of exciton binding energies in monolayer WS₂,” *Phys. Rev. Lett.* **115**, 126802 (2015).
58. Z. Wang et al., “Greatly enhanced resonant exciton-trion conversion in electrically modulated atomically thin WS₂ at room temperature,” *Adv. Mater.* **35**, 2302248 (2023).
59. P. Back et al., “Realization of an electrically tunable narrow-bandwidth atomically thin mirror using monolayer MoSe₂,” *Phys. Rev. Lett.* **120**, 037401 (2018).
60. Y. Zhou et al., “Controlling excitons in an atomically thin membrane with a mirror,” *Phys. Rev. Lett.* **124**, 027401 (2020).
61. M. Li et al., “Excitonic beam steering in an active van der Waals metasurface,” *Nano Lett.* **23**, 2771–2777 (2023).
62. J. van de Groep et al., “Exciton resonance tuning of an atomically thin lens,” *Nat. Photonics* **14**, 426–430 (2020).
63. Q. Li et al., “A Purcell-enabled monolayer semiconductor free-space optical modulator,” *Nat. Photonics* **17**, 897–903 (2023).
64. T. Low et al., “Polaritons in layered two-dimensional materials,” *Nat. Mater.* **16**, 182–194 (2017).
65. Q. Xu et al., “Meta-optics inspired surface plasmon devices,” *Photonics Insights* **2**, R02 (2023).
66. F. Xia et al., “Two-dimensional material nanophotonics,” *Nat. Photonics* **8**, 899–907 (2014).
67. H. Xin, B. Namgung, and L. P. Lee, “Nanoplasmonic optical antennas for life sciences and medicine,” *Nat. Rev. Mater.* **3**, 228–243 (2018).
68. N. Jiang, X. Zhuo, and J. Wang, “Active plasmonics: principles, structures, and applications,” *Chem. Rev.* **118**, 3054–3099 (2018).
69. N. I. Zheludev and G. Yuan, “Optical superoscillation technologies beyond the diffraction limit,” *Nat. Rev. Phys.* **4**, 16–32 (2022).
70. F. H. L. Koppens, D. E. Chang, and F. J. García de Abajo, “Graphene plasmonics: a platform for strong light-matter interactions,” *Nano Lett.* **11**, 3370–3377 (2011).
71. Z. Fei et al., “Gate-tuning of graphene plasmons revealed by infrared nano-imaging,” *Nature* **487**, 82–85 (2012).
72. J. Chen et al., “Optical nano-imaging of gate-tunable graphene plasmons,” *Nature* **487**, 77–81 (2012).
73. L. Wang and X. G. Xu, “Scattering-type scanning near-field optical microscopy with reconstruction of vertical interaction,” *Nat. Commun.* **6**, 8973 (2015).
74. A. Woessner et al., “Highly confined low-loss plasmons in graphene–boron nitride heterostructures,” *Nat. Mater.* **14**, 421–425 (2015).
75. G. X. Ni et al., “Fundamental limits to graphene plasmonics,” *Nature* **557**, 530–533 (2018).
76. J. Nong et al., “Enhanced graphene plasmonic mode energy for highly sensitive molecular fingerprint retrieval,” *Laser Photonics Rev.* **15**, 2000300 (2021).

77. Z. Fang et al., "Active tunable absorption enhancement with graphene nanodisk arrays," *Nano Lett.* **14**, 299–304 (2014).
78. D. Rodrigo et al., "Double-layer graphene for enhanced tunable infrared plasmonics," *Light Sci. Appl.* **6**, e16277 (2017).
79. H. Yan et al., "Damping pathways of mid-infrared plasmons in graphene nanostructures," *Nat. Photonics* **7**, 394–399 (2013).
80. V. W. Brar et al., "Electronic modulation of infrared radiation in graphene plasmonic resonators," *Nat. Commun.* **6**, 7032 (2015).
81. S. Kim et al., "Electronically tunable extraordinary optical transmission in graphene plasmonic ribbons coupled to subwavelength metallic slit arrays," *Nat. Commun.* **7**, 12323 (2016).
82. D. Rodrigo et al., "Mid-infrared plasmonic biosensing with grapheme," *Science* **349**, 165–168 (2015).
83. H. Hu et al., "Far-field nanoscale infrared spectroscopy of vibrational fingerprints of molecules with graphene plasmons," *Nat. Commun.* **7**, 12334 (2016).
84. Q. Guo et al., "Efficient electrical detection of mid-infrared graphene plasmons at room temperature," *Nat. Mater.* **17**, 986–992 (2018).
85. T. Sun et al., "Graphene plasmonic nanoresonators/graphene heterostructures for efficient room-temperature infrared photodetection," *J. Semicond.* **41**, 072907 (2020).
86. Z. Fei et al., "Tunneling plasmonics in bilayer grapheme," *Nano Lett.* **15**, 4973–4978 (2015).
87. T. Huang et al., "Observation of chiral and slow plasmons in twisted bilayer grapheme," *Nature* **605**, 63–68 (2022).
88. S. Zhang et al., "Visualizing moiré ferroelectricity via plasmons and nano-photocurrent in graphene/twisted-WSe₂ structures," *Nat. Commun.* **14**, 6200 (2023).
89. I.-H. Lee et al., "Anisotropic acoustic plasmons in black phosphorus," *ACS Photonics* **5**, 2208–2216 (2018).
90. X. Huang et al., "Black phosphorus carbide as a tunable anisotropic plasmonic metasurface," *ACS Photonics* **5**, 3116–3123 (2018).
91. M. Zhao et al., "Electrostatically tunable near-infrared plasmonic resonances in solution-processed atomically thin NbSe₂," *Adv. Mater.* **33**, 2101950 (2021).
92. X. Guo et al., "Studying plasmon dispersion of MXene for enhanced electromagnetic absorption," *Adv. Mater.* **34**, 2201120 (2022).
93. C. Lian et al., "Integrated plasmonics: broadband Dirac plasmons in borophene," *Phys. Rev. Lett.* **125**, 116802 (2020).
94. J. Nong et al., "Effective transmission modulation at telecommunication wavelengths through continuous metal films using coupling between borophene plasmons and magnetic polaritons," *Adv. Opt. Mater.* **9**, 2001809 (2021).
95. J. Nong et al., "Active modulation of graphene near-infrared electroabsorption employing borophene plasmons in a wide waveband," *Adv. Opt. Mater.* **10**, 2102131 (2022).
96. C. Song et al., "Plasmons in the van der Waals charge-density-wave material 2H-TaSe₂," *Nat. Commun.* **12**, 386 (2021).
97. P. Cudazzo et al., "Negative plasmon dispersion in 2H-NbS₂ beyond the charge-density-wave interpretation," *New J. Phys.* **18**, 103050 (2016).
98. V. Pacheco-Peña, T. Hallam, and N. Healy, "MXene supported surface plasmons on telecommunications optical fibers," *Light Sci. Appl.* **11**, 22 (2022).
99. S. G. Menabde et al., "Near-field probing of image phonon-polaritons in hexagonal boron nitride on gold crystals," *Sci. Adv.* **8**, eabn0627 (2022).
100. A. J. Giles et al., "Ultralow-loss polaritons in isotopically pure boron nitride," *Nat. Mater.* **17**, 134–139 (2018).
101. M. Tamagnone et al., "Ultra-confined mid-infrared resonant phonon polaritons in van der Waals nanostructures," *Sci. Adv.* **4**, eaat7189 (2018).
102. J. Duan et al., "Active and passive tuning of ultranarrow resonances in polaritonic nanoantennas," *Adv. Mater.* **34**, 2104954 (2022).
103. H. Hu et al., "Doping-driven topological polaritons in graphene/ α -MoO₃ heterostructures," *Nat. Nanotechnol.* **17**, 940–946 (2022).
104. W. Ma et al., "In-plane anisotropic and ultra-low-loss polaritons in a natural van der Waals crystal," *Nature* **562**, 557–562 (2018).
105. G. Hu et al., "Topological polaritons and photonic magic angles in twisted α -MoO₃ bilayers," *Nature* **582**, 209–213 (2020).
106. M. Chen et al., "Configurable phonon polaritons in twisted α -MoO₃," *Nat. Mater.* **19**, 1307–1311 (2020).
107. S. G. Menabde et al., "Low-loss anisotropic image polaritons in van der Waals crystal α -MoO₃," *Adv. Opt. Mater.* **10**, 2201492 (2022).
108. J. Yang et al., "High- Q phonon-polaritons in spatially confined freestanding α -MoO₃," *ACS Photonics* **9**, 905–913 (2022).
109. Y. Cao et al., "Correlated insulator behaviour at half-filling in magic-angle graphene superlattices," *Nature* **556**, 80–84 (2018).
110. M. Kauranen and A. V. Zayats, "Nonlinear plasmonics," *Nat. Photonics* **6**, 737–748 (2012).
111. K. Koshelev, A. Bogdanov, and Y. Kivshar, "Meta-optics and bound states in the continuum," *Sci. Bull.* **64**, 836–842 (2019).
112. P. Vabishchevich and Y. Kivshar, "Nonlinear photonics with metasurfaces," *Photonics Res.* **11**, B50–B64 (2023).
113. Z. Sun, T. Hasan, and A. C. Ferrari, "Ultrafast lasers mode-locked by nanotubes and grapheme," *Phys. E Low-Dimens. Syst. Nanostruct.* **44**, 1082–1091 (2012).
114. A. Säynätjoki et al., "Rapid large-area multiphoton microscopy for characterization of grapheme," *ACS Nano* **7**, 8441–8446 (2013).
115. E. Hendry et al., "Coherent nonlinear optical response of grapheme," *Phys. Rev. Lett.* **105**, 097401 (2010).
116. R. Wu et al., "Purely coherent nonlinear optical response in solution dispersions of graphene sheets," *Nano Lett.* **11**, 5159–5164 (2011).
117. D. Sun et al., "Coherent control of ballistic photocurrents in multilayer epitaxial graphene using quantum interference," *Nano Lett.* **10**, 1293–1296 (2010).
118. J. Wang et al., "Broadband nonlinear optical response of graphene dispersions," *Adv. Mater.* **21**, 2430–2435 (2009).
119. H. Yang et al., "Giant two-photon absorption in bilayer grapheme," *Nano Lett.* **11**, 2622–2627 (2011).
120. J. J. Dean and H. M. van Driel, "Second harmonic generation from graphene and graphitic films," *Appl. Phys. Lett.* **95**, 261910 (2009).
121. J. J. Dean and H. M. van Driel, "Graphene and few-layer graphite probed by second-harmonic generation: theory and experiment," *Phys. Rev. B* **82**, 125411 (2010).
122. K. Wang et al., "Ultrafast saturable absorption of two-dimensional MoS₂ nanosheets," *ACS Nano* **7**, 9260–9267 (2013).
123. Y. Li et al., "Probing symmetry properties of few-layer MoS₂ and h-BN by optical second-harmonic generation," *Nano Lett.* **13**, 3329–3333 (2013).
124. A. Säynätjoki et al., "Ultra-strong nonlinear optical processes and trigonal warping in MoS₂ layers," *Nat. Commun.* **8**, 893 (2017).
125. C. Janisch et al., "Ultrashort optical pulse characterization using WS₂ monolayers," *Opt. Lett.* **39**, 383–385 (2014).
126. H. Liu et al., "High-harmonic generation from an atomically thin semiconductor," *Nat. Phys.* **13**, 262–265 (2017).
127. N. Dong et al., "Optical limiting and theoretical modelling of layered transition metal dichalcogenide nanosheets," *Sci. Rep.* **5**, 14646 (2015).
128. T. Jakubczyk et al., "Radiatively limited dephasing and exciton dynamics in MoSe₂ monolayers revealed with four-wave mixing microscopy," *Nano Lett.* **16**, 5333–5339 (2016).
129. X. Xu et al., "Spin and pseudospins in layered transition metal dichalcogenides," *Nat. Phys.* **10**, 343–350 (2014).
130. J. Qiao et al., "High-mobility transport anisotropy and linear dichroism in few-layer black phosphorus," *Nat. Commun.* **5**, 4475 (2014).

131. N. Youngblood et al., “Layer-tunable third-harmonic generation in multilayer black phosphorus,” *ACS Photonics* **4**, 8–14 (2017).
132. J. Zheng et al., “Black phosphorus based all-optical-signal-processing: toward high performances and enhanced stability,” *ACS Photonics* **4**, 1466–1476 (2017).
133. G. Hu et al., “Black phosphorus ink formulation for inkjet printing of optoelectronics and photonics,” *Nat. Commun.* **8**, 278 (2017).
134. Y. Y. Illarionov et al., “Long-term stability and reliability of black phosphorus field-effect transistors,” *ACS Nano* **10**, 9543–9549 (2016).
135. T. T. Tran et al., “Quantum emission from hexagonal boron nitride monolayers,” *Nat. Nanotechnol.* **11**, 37–41 (2016).
136. H. Wang and X. Qian, “Giant optical second harmonic generation in two-dimensional multiferroics,” *Nano Lett.* **17**, 5027–5034 (2017).
137. A. K. Geim and I. V. Grigorieva, “Van der Waals heterostructures,” *Nature* **499**, 419–425 (2013).
138. D. Li et al., “Multimodal nonlinear optical imaging of MoS₂ and MoS₂-based van der Waals heterostructures,” *ACS Nano* **10**, 3766–3775 (2016).
139. H. Chen et al., “Transition-metal dichalcogenides heterostructure saturable absorbers for ultrafast photonics,” *Opt. Lett.* **42**, 4279–4282 (2017).
140. M. L. Brongersma, “The road to atomically thin metasurface optics,” *Nanophotonics* **10**, 643–654 (2021).
141. A. A. Popkova et al., “Nonlinear exciton-Mie coupling in transition metal dichalcogenide nanoresonators,” *Laser Photonics Rev.* **16**, 2100604 (2022).
142. M. Panmai et al., “Revealing Mie resonances with enhanced and suppressed second-order nonlinear optical responses in a hexagonal-prism-like MoS₂ nanoparticle,” *Laser Photonics Rev.* **17**, 2300346 (2023).
143. G. Zograf et al., “Combining ultrahigh index with exceptional nonlinearity in resonant transition metal dichalcogenide nanodisks,” arXiv:2308.11504 (2023).
144. R. Biswas et al., “Enhanced four wave mixing from MoS₂ disks supporting higher-order anapole resonance,” *Proc. SPIE* **12423**, 1242308 (2023).
145. M. Nauman et al., “Tunable unidirectional nonlinear emission from transition-metal-dichalcogenide metasurfaces,” *Nat. Commun.* **12**, 5597 (2021).
146. J. Shi et al., “Giant enhancement and directional second harmonic emission from monolayer WS₂ on silicon substrate via Fabry-Pérot micro-cavity,” *ACS Nano* **16**, 13933–13941 (2022).
147. J. Du et al., “An on-Si directional second harmonic generation amplifier for MoS₂/WS₂ heterostructure,” *Nano Res.* **16**, 4061–4066 (2023).
148. L. Kühner et al., “High-*Q* nanophotonics over the full visible spectrum enabled by hexagonal boron nitride metasurfaces,” *Adv. Mater.* **35**, 2209688 (2023).
149. F. J. F. Löchner et al., “Hybrid dielectric metasurfaces for enhancing second-harmonic generation in chemical vapor deposition grown MoS₂ monolayers,” *ACS Photonics* **8**, 218–227 (2021).
150. Z. Liu et al., “Giant enhancement of continuous wave second harmonic generation from few-layer GaSe coupled to high-*Q* quasi bound states in the continuum,” *Nano Lett.* **21**, 7405–7410 (2021).
151. N. Bernhardt et al., “Quasi-BIC resonant enhancement of second-harmonic generation in WS₂ monolayers,” *Nano Lett.* **20**, 5309–5314 (2020).
152. E. Mikheeva et al., “Space and time modulations of light with metasurfaces: recent progress and future prospects,” *ACS Photonics* **9**, 1458–1482 (2022).
153. M. Hentschel et al., “Dielectric Mie voids: confining light in air,” *Light Sci. Appl.* **12**, 3 (2023).
154. C.-H. Liu et al., “Developing ultrathin light emitters and metalenses based on van der Waals materials,” *Proc. SPIE* **10920**, 1092005 (2019).
155. P. Tonkaev et al., “Multifunctional and transformative metaphotonics with emerging materials,” *Chem. Rev.* **122**, 15414–15449 (2022).
156. F. Qin et al., “ π -phase modulated monolayer supercritical lens,” *Nat. Commun.* **12**, 32 (2021).
157. S.-W. Moon et al., “Recent progress on ultrathin metalenses for flat optics,” *iScience* **23**, 101877 (2020).
158. Y. Peng et al., “Metalens in improving imaging quality: advancements, challenges, and prospects for future display,” *Laser Photonics Rev.* **18**, 2300731 (2024).
159. X. Wang, Y. Sun, and K. Liu, “Chemical and structural stability of 2D layered materials,” *2D Mater.* **6**, 042001 (2019).
160. J. Gao et al., “Aging of transition metal dichalcogenide monolayers,” *ACS Nano* **10**, 2628–2635 (2016).
161. Q. Zhou et al., “Light-induced ambient degradation of few-layer black phosphorus: mechanism and protection,” *Angew. Chem. Int. Ed.* **55**, 11437–11441 (2016).
162. Z. Hu et al., “Water-catalyzed oxidation of few-layer black phosphorous in a dark environment,” *Angew. Chem. Int. Ed.* **56**, 9131–9135 (2017).
163. W. Huang et al., “Encapsulation strategies on 2D materials for field effect transistors and photodetectors,” *Chin. Chem. Lett.* **33**, 2281–2290 (2022).
164. G. Long et al., “Type-controlled nanodevices based on encapsulated few-layer black phosphorus for quantum transport,” *2D Mater.* **3**, 031001 (2016).
165. X. Chen et al., “High-quality sandwiched black phosphorus heterostructure and its quantum oscillations,” *Nat. Commun.* **6**, 7315 (2015).
166. S. A. Wells et al., “Suppressing ambient degradation of exfoliated InSe nanosheet devices via seeded atomic layer deposition encapsulation,” *Nano Lett.* **18**, 7876–7882 (2018).
167. X. Hu et al., “Halide-induced self-limited growth of ultrathin nonlayered Ge flakes for high-performance phototransistors,” *J. Am. Chem. Soc.* **140**, 12909–12914 (2018).
168. J. Jia et al., “Plasma-treated thickness-controlled two-dimensional black phosphorus and its electronic transport properties,” *ACS Nano* **9**, 8729–8736 (2015).
169. G. Wang et al., “Introduction of interfacial charges to black phosphorus for a family of planar devices,” *Nano Lett.* **16**, 6870–6878 (2016).
170. Y. L. Huang et al., “The organic–2D transition metal dichalcogenide heterointerface,” *Chem. Soc. Rev.* **47**, 3241–3264 (2018).
171. J. Sun et al., “2D–organic hybrid heterostructures for optoelectronic applications,” *Adv. Mater.* **31**, 1803831 (2019).
172. K. Kang et al., “High-mobility three-atom-thick semiconducting films with wafer-scale homogeneity,” *Nature* **520**, 656–660 (2015).
173. Y.-H. Lee et al., “Synthesis of large-area MoS₂ atomic layers with chemical vapor deposition,” *Adv. Mater.* **24**, 2320–2325 (2012).
174. S. Heiserer et al., “Controllable and reproducible growth of transition metal dichalcogenides by design of experiments,” *Adv. Electron. Mater.* **9**, 2300281 (2023).
175. Y. Zhang et al., “Experimental observation of the quantum Hall effect and Berry’s phase in graphene,” *Nature* **438**, 201–204 (2005).
176. K. S. Novoselov et al., “Electric field effect in atomically thin carbon films,” *Science* **306**, 666–669 (2004).
177. A. K. Geim and K. S. Novoselov, “The rise of graphene,” *Nat. Mater.* **6**, 183–191 (2007).
178. V. Nicolosi et al., “Liquid exfoliation of layered materials,” *Science* **340**, 1226419 (2013).
179. J. N. Coleman et al., “Two-dimensional nanosheets produced by liquid exfoliation of layered materials,” *Science* **331**, 568–571 (2011).
180. K. R. Paton et al., “Scalable production of large quantities of defect-free few-layer graphene by shear exfoliation in liquids,” *Nat. Mater.* **13**, 624–630 (2014).

181. Z. Lin et al., "Solution-processable 2D semiconductors for high-performance large-area electronics," *Nature* **562**, 254–258 (2018).
182. J. Li et al., "Printable two-dimensional superconducting monolayers," *Nat. Mater.* **20**, 181–187 (2021).
183. S. Liu et al., "Nanopatterning technologies of 2D materials for integrated electronic and optoelectronic devices," *Adv. Mater.* **34**, 2200734 (2022).
184. P. S. Kollipara, J. Li, and Y. Zheng, "Optical patterning of two-dimensional materials," *Research* **2020**, 6581250 (2020).

Zeng Wang earned his doctorate from the School of Physical and Mathematical Sciences at Nanyang Technological University in Singapore. He now holds the position of senior scientist at the Institute of Materials Research and Engineering (IMRE), under the Agency for Science, Technology and Research (A*STAR). His research focuses on metaoptics, 2D optoelectronics, and advanced high-resolution optical lithography techniques.

Kandammathe Valiyaveedu Sreekanth is currently a senior scientist in the Institute of Materials Research and Engineering (IMRE), A*STAR, Singapore. He received his PhD from Nanyang Technological University, Singapore. His research interests include nanophotonics, metasurfaces, phase-change materials, and biosensors.

Meng Zhao received her PhD from National University of Singapore (NUS) in 2014. She is currently a senior scientist in the Institute of Materials Research and Engineering (IMRE), A*STAR, Singapore. Her current research interests focus mainly on the preparation and optoelectronics of novel 2D materials.

Jinpeng Nong received his PhD from the College of Optoelectronic Engineering, Chongqing University, China. He is currently a senior scientist in the Institute of Materials Research and Engineering (IMRE), A*STAR. His research interests include plasmonics and nanophotonics, 2D optoelectronics, mid-IR spectroscopy, and photodetection.

Yincheng Liu received his bachelor of arts degree from University of Oxford. He is currently a research engineer in the Institute of Materials Research and Engineering (IMRE), A*STAR. He is currently working on characterization of optoelectronic devices made of 2D materials.

Jinghua Teng received his PhD from the Department of Electrical and Computer Engineering, National University of Singapore. He is currently a senior principal scientist and senior group leader in the Institute of Materials Research and Engineering (IMRE), A*STAR. His research interests include nanophotonics, metamaterials and metasurfaces, 2D optoelectronics, and terahertz technology.